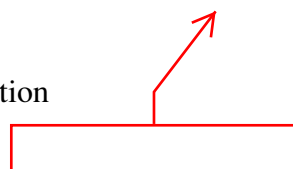


## Metadata of the chapter that will be visualized online

Chapter Title	Remote Sensing of Vegetation: Potentials, Limitations, Developments and Applications
Copyright Year	2015
Copyright Holder	Springer Science+Business Media Dordrecht
Corresponding Author	Family Name <b>Mathias Disney</b> Particle Given Name Suffix Division Department of Geography Organization University College London, <del>Geography</del> Address Gower Street, London WC1E 6BT, UK Organization NERC National Centre for Earth Observation Address <del>Didcot, UK</del> Email mathias.disney@ucl.ac.uk



**Abstract** Earth observation, i.e., gaining information of Earth's physical, chemical and biological characteristics by remote sensing methods, can be used to make a range of quantitative measurements related to vegetation canopy structure and function. The capabilities of Earth observation for mapping, even indirectly, canopy state and function over wide areas and over decadal time-scales allow for studies of phenology, disturbance, anthropogenic impacts and responses to climate change. Key limitations of Earth observation measurements are discussed, in particular how their indirect nature makes them potentially hard to interpret and relate to physically-measurable quantities, as well as assumptions that are made to derive information from Earth observation data. Various Earth observation measurements of vegetation routinely provided from satellite data are introduced and a radiative transfer framework for developing, understanding and exploiting these measurements is outlined. This framework is critical in that it allow us to chart a consistent route from measurements made at the top-of-the atmosphere to estimates of canopy state and function. The impacts of assumptions required to solve the canopy radiative transfer problem in practical applications are discussed. New developments in radiative transfer theory and modelling are introduced, in particular focusing on how incorporating the vegetation structure in these models is key to interpreting many Earth observation measurements. These new techniques help to unpick the nature of the canopy signal from Earth observation measurements. The (key) issue of 'effective' model parameters that are often used to interpret and exploit observations is raised. These simplified or approximate manifestations of measurable physical properties permit development of practical, rapid models of the sort required for global applications but potentially introduce inconsistency between Earth observation measurements and models of vegetation productivity. Methods to overcome these limitations are discussed, such as data assimilation, which is being used to provide consistent model-data

frameworks and make best use of both. Lastly, new remote sensing measurements are described that are providing information on 3D canopy structure, from lidar particularly, and canopy function from fluorescence. These measurements, along with other Earth observation data and model-data fusion techniques are providing new insights into canopy state and function on global scales.

---

# Chapter 11

## Remote Sensing of Vegetation: Potentials, Limitations, Developments and Applications

Mathias Disney\*

Department of Geography, University College London, ~~Geography~~, Gower Street,  
London WC1E 6BT, UK

NERC National Centre for Earth Observation, ~~Didcot~~, UK

6	Summary .....	1
7	I. Introduction .....	3
8	A. What Is Earth Observation? .....	3
9	B. What Earth Observation Can and Can't Measure .....	3
10	II. Radiative Transfer in Vegetation: The Problem and Some Solutions .....	8
11	A. Statement of the Radiative Transfer Problem .....	8
12	B. Solving the Radiative Transfer Problem for Explicit Canopy Structure .....	10
13	C. Radiation Transfer Within the Leaf .....	16
14	D. Recollision Probability and Spectral Invariance .....	18
15	E. 3D Monte Carlo Approaches .....	20
16	III. Effective Parameters .....	23
17	A. Basics: Definition of Effective Characteristics .....	23
18	B. Data Assimilation .....	23
19	C. Scale Differences and Model Intercomparisons .....	24
20	IV. New Observations of Structure and Function .....	26
21	A. Structural Information from Lidar and RADAR .....	26
	1. Discrete-Return Lidar Systems .....	27
	2. Full-Waveform Lidar Systems .....	27
	3. Limitations and Future Developments of Lidar Systems .....	27
	4. Terrestrial Laser Scanning (TLS) .....	29
	5. RADAR Systems .....	32
22	B. Fluorescence and Canopy Function .....	32
23	V. Conclusions .....	35
24	Acknowledgments .....	35
25	References .....	36

### 26 Summary

28 Earth observation, i.e., gaining information of Earth's physical, chemical and biological  
 29 characteristics by remote sensing methods, can be used to make a range of quantitative  
 30 measurements related to vegetation canopy structure and function. The capabilities of Earth  
 31 observation for mapping, even indirectly, canopy state and function over wide areas and over  
 32 decadal time-scales allow for studies of phenology, disturbance, anthropogenic impacts and

---

\*Author for correspondence, e-mail: [mathias.disney@ucl.ac.uk](mailto:mathias.disney@ucl.ac.uk)

33 responses to climate change. Key limitations of Earth observation measurements are  
 34 discussed, in particular how their indirect nature makes them potentially hard to interpret  
 35 and relate to physically-measurable quantities, as well as assumptions that are made to derive  
 36 information from Earth observation data. Various Earth observation measurements of  
 37 vegetation routinely provided from satellite data are introduced and a radiative transfer  
 38 framework for developing, understanding and exploiting these measurements is outlined.  
 39 This framework is critical in that it allow us to chart a consistent route from measurements  
 40 made at the top-of-the atmosphere to estimates of canopy state and function. The impacts of  
 41 assumptions required to solve the canopy radiative transfer problem in practical applications  
 42 are discussed. New developments in radiative transfer theory and modelling are introduced, in  
 43 particular focusing on how incorporating the vegetation structure in these models is key to  
 44 interpreting many Earth observation measurements. These new techniques help to unpick the  
 45 nature of the canopy signal from Earth observation measurements. The (key) issue of ‘effective’  
 46 model parameters that are often used to interpret and exploit observations is raised. These  
 47 simplified or approximate manifestations of measurable physical properties permit develop-  
 48 ment of practical, rapid models of the sort required for global applications but potentially  
 49 introduce inconsistency between Earth observation measurements and models of vegetation  
 50 productivity. Methods to overcome these limitations are discussed, such as data assimilation,  
 51 which is being used to provide consistent model-data frameworks and make best use of both.  
 52 Lastly, new remote sensing measurements are described that are providing information on 3D

---

*Abbreviations:*  $A_l$  – Area of a given leaf; ALS – Airborne laser scanning; BRDF – Bidirectional reflectance distribution function;  $c$  – Speed of light;  $d$  – Sensor-target distance; DA – Data assimilation; DASF – Directional area scattering factor; DEM – Digital elevation model; DGVM – Dynamic global vegetation model; DWEL – Dual-wavelength Echidna laser scanner;  $E_i$  – Downwelling surface irradiance; EO – Earth observation; ESA – European Space Agency; ESM – Earth system model; ESS – Earth system science; EVI – Enhanced vegetation index; fAPAR – Fraction of absorbed photosynthetically active radiation;  $F_s$  – Solar-induced chlorophyll fluorescence; FTS – Fourier Transform Spectrometer;  $g_l(z, \Omega_l)$  – Angular distribution of leaf normal vectors (leaf angle distribution);  $G_l(\Omega)$ ,  $G_l(\Omega')$  – Leaf projection function in direction  $\Omega$ ,  $\Omega'$  respectively; GLAS – Geoscience Laser Altimeter System; GO – Geometric optics; GOSAT – Greenhouse Gases Observing Satellite; GPP – Gross primary productivity;  $h_l(\phi_l)$  – Azimuthal dependence of leaf angle,  $\phi_l$ ;  $H$  – Canopy total height;  $H(x)$  – Observation operator, mapping model state variable vector  $x$  to the EO signal;  $i_0$  – Radiation first intercepted in the canopy by leaves;  $i_L$  – Leaf interceptance that enters the leaf interior;  $I_r$  – Upwelling (reflected) radiance;  $I(z, \Omega)$  – Specific energy intensity in direction  $\Omega$  at depth  $z$  in a horizontal plane-parallel canopy;  $J_s(z, \Omega')$  – Source term of radiative transfer equation at depth  $z$ , in direction  $\Omega'$ ;  $\kappa_c$  – Volume extinction coefficient;  $L(z)$  – Cumulative leaf area index at depth  $z$ ; LAD – Leaf angle distribution; LAI – Leaf area index;  $LAI$  – Effective LAI; lidar – Light detection and ranging; LSM – Land surface

---

model; MCRT – Monte Carlo ray tracing; MERIS – Medium Resolution Imaging Spectrometer; MISR – Multiangle Imaging Spectroradiometer; MODIS – Moderate Resolution Imaging Spectroradiometer;  $N$  – Number of leaves per unit volume; NASA – National Aeronautics and Space Administration; NDVI – Normalized difference vegetation index; NIR – Near infrared; NPP – Net primary productivity;  $p$  – Recollision probability;  $P(z, \Omega' \rightarrow \Omega)$  – Volume scattering phase function; PFT – Plant functional type; PILPS – Project for Intercomparison of Land Surface Parameterization Schemes;  $Q_0$  – Uncollided radiation passing through the canopy to the lower boundary layer;  $\mathbf{R}$  – Vector of EO measurements; RADAR – Radio detection and ranging; RAMI – Radiation Transfer Model Intercomparison;  $\mathbf{S}$  – Radiation model system state vector; SALCA – Salford Advanced Laser Canopy Analyser; SWIR – Shortwave infrared;  $t$  – Time of flight; TANSO – Thermal and Near infrared Sensor for carbon Observation; TLS – Terrestrial laser scanning;  $z$  – Canopy depth;  $\mathbf{Z}$  – Radiation signal modelled by a radiation model with state variable  $\mathbf{S}$ ;  $W_\lambda$  – Spectral canopy scattering coefficient;  $\zeta$  – Canopy clumping factor;  $\lambda$  – Wavelength;  $\mu$ ,  $\mu'$  – Cosine of the view, illumination direction vectors  $\Omega$ ,  $\Omega'$  with the local normal;  $\rho$  – Reflectance;  $\tau$  – Transmittance;  $\theta_{v,i}$  – View, illumination zenith angles;  $\varphi_{v,i}$  – View, illumination azimuth angles;  $u_l(z)$  – Canopy leaf area density at depth  $z$ ;  $\omega$  – Leaf single scattering albedo;  $\hat{\omega}_\lambda$  – Spectral leaf single scattering albedo normalized by leaf interceptance;  $\Omega(\theta_v, \varphi_v)$  and  $\Omega'(\theta_i, \varphi_i)$  – View, illumination vectors

53 canopy structure, from lidar particularly, and canopy function from fluorescence. These  
 54 measurements, along with other Earth observation data and model-data fusion techniques  
 55 are providing new insights into canopy state and function on global scales.

## I. Introduction

### A. What Is Earth Observation?

56 Terrestrial vegetation is a key component of  
 57 the Earth's climate system, via mediation  
 58 of fluxes of solar radiation, water and atmo-  
 59 spheric gases at the land surface, and  
 60 the resulting interactions with and feedback  
 61 to the global carbon cycle (Denman  
 62 et al. 2008). Terrestrial vegetation processes  
 63 operate across a huge range of time-scales,  
 64 responding at seconds to hourly and daily  
 65 time-scales to changes in environmental  
 66 conditions temperature, precipitation and  
 67 light, and in seasonal and much longer  
 68 time-scales to cycles of climate and global  
 69 change. Vegetation is also heterogeneous at a  
 70 huge range of scales (within leaf, root  
 71 systems) to composition of savannahs and  
 72 forests shaped by millennia of evolutionary,  
 73 climate and more recently anthropogenic  
 74 influences. Vegetation is of course also inti-  
 75 mately connected to human activity in provi-  
 76 sion of food, shelter, fuel and many other  
 77 direct and indirect ecosystem services.

78 The importance of understanding the state  
 79 and function of vegetation has led to develop-  
 80 ment of a wide range of observational and  
 81 modelling techniques (e.g. Wang 2004; Monteith  
 82 and Unsworth 2008; Jones 2014). Of these,  
 83 remote sensing (hereafter referred to as Earth  
 84 observation (EO), to distinguish it from plan-  
 85 etary remote sensing) has become a central  
 86 part of efforts to address many of these issues  
 87 due to the large spatiotemporal scales that can  
 88 be covered by satellite and airborne  
 89 instruments. The developments of EO have  
 90 seen huge advances in instrument design,  
 91 accuracy, consistency and the ability to han-  
 92 dle large (and ever-growing) datasets (Lynch  
 93 2008). These benefits have led to EO becom-  
 94 ing ubiquitous in Earth System Science. A  
 95 wide range of problems at global and regional  
 96 scales are ideally-suited to the scale and cov-  
 97 erage of EO. New observations and models  
 98 have arisen in tandem, sometimes by design,

although more often not. This has led to many  
 new developments for exploiting EO data in  
 understanding and measuring the Earth Sys-  
 tem (Chapin et al. 2011). This has also raised  
 fundamental questions about how such  
 observations can be used (Pfeifer et al. 2012).

Here, I introduce the problem of how EO  
 can be used for understanding and quantifying  
 terrestrial vegetation i.e. what can and  
 can't be measured via EO. A key advantage  
 of remote sensing, its remoteness, is also a  
 key limitation: what we actually *can* measure  
 is rarely what we *want* to measure. To trans-  
 late the former to the latter, a hierarchy of  
 models has been developed. I outline some  
 of the issues and approaches to modelling  
 across this hierarchy: from scattering and  
 absorption of radiation (EO models),  
 through models that transform radiation  
 into canopy properties (state, productivity,  
 dynamics) and on to large-scale models of  
 ecosystem processes, both of the current  
 state (diagnostic, biogeochemical cycling)  
 and future changes (prognostic, dynamic  
 global vegetation models (DGVMS), and  
 their big brothers, global climate models).  
 If and when these various models interface  
 with EO data, they do so in very different  
 ways due to their underlying assumptions,  
 structure and aims. I discuss some of the  
 consequences of these variations (and  
 inconsistencies) from the point of view of  
 how EO can be used to understand and quan-  
 tify terrestrial vegetation systems, as well  
 as how models may be developed to better  
 exploit EO data. Clearly, quantifying the  
 state of terrestrial ecosystems and under-  
 standing how they will change in the face  
 of uncertain climate and anthropogenic  
 drivers, requires best use of both observa-  
 tions and models.

### B. What Earth Observation Can and Can't Measure

The value of an EO measurement is simply  
 the answer to the question: how much

144 information about the system being observed  
 145 is contained within the EO measurement of  
 146 that system? The EO signal is a measure of  
 147 scattered (reflected, transmitted) or emitted  
 148 radiation from a target. We measure photons  
 149 escaping towards a sensor, from a target,  
 150 either above the atmosphere in the case of a  
 151 satellite, or at some point lower down in the  
 152 case of airborne or even ground-based  
 153 observations. Table 11.1 describes a list of  
 154 properties that EO can and does provide,  
 155 along with an assessment of the level of  
 156 how ‘direct’ these measurements are in  
 157 some sense, from the perspective of any  
 158 additional ground-level measurements or  
 159 modelling needed to interpret the  
 160 measurements. Not surprisingly, as EO  
 161 ‘measurements’ become less direct, three  
 162 critical (and related) things occur:

- 163 • The number of assumptions underlying an EO  
 164 measurement becomes larger and the oppor-  
 165 tunity for these assumptions to become incon-  
 166 sistent at some level increases.
- 167 • The uncertainty associated with an EO mea-  
 168 surement becomes more difficult to quantify  
 169 (albeit not necessarily larger), due to the  
 170 increasing number of assumptions and  
 171 requirements for ancillary information, and  
 172 the way uncertainties in each may combine  
 173 in potentially non-linear ways.
- 174 • The more difficult it is likely to be to compare  
 175 an EO measurement against independent  
 176 measurements (or model-derived estimates)  
 177 of what ought to be the same property. This  
 178 is due to possible differences in underpinning  
 179 assumptions and ancillary information.

181 These issues of the limits of remote sens-  
 182 ing measurement are identified by Verstraete  
 183 et al. (1996). They define a physical model  
 184 relationship between an observation of emit-  
 185 ted radiation  $Z$  and a system described by  
 186 model state variables  $S$  as

$$Z = fS \quad (11.1)$$

187 where the  $S$  are the smallest set of variables  
 188 needed to fully describe the physical state of  
 189 the observed system, at the scale of

observation. It is worth repeating the first  
 190 proposition of Verstraete et al. (1996) on  
 191 the limitations of remote sensing, as it  
 192 provides a useful framing for the ensuing  
 193 discussion: “A physical interpretation of  
 194 electromagnetic measurements  $Z$  obtained  
 195 from remote sensing can provide reliable  
 196 quantitative information *only on the radia-  
 197 tive state variables  $S$  that control the emis-  
 198 sion of radiation from its source and its  
 199 interaction with all intervening media and  
 200 the detector*” (emphasis added). We may be  
 201 able to translate from  $S$  to other parameters  
 202 of interest that may rely on  $S$  indirectly  
 203 (e.g. canopy state or function), but we always  
 204 require a mapping back to  $S$  at some point if  
 205 we wish to make use of remote sensing.  
 206

The last category in Table 11.1 is intended  
 207 to indicate properties that are either not well-  
 208 defined (i.e. do not have a clear physically-  
 209 derived meaning), or perhaps are not directly  
 210 measurable quantities i.e. in the formalism  
 211 of Verstraete et al. (1996) we are not able to  
 212 define a physically-based mapping  $Z = f(S)$   
 213 for these parameters. However, such  
 214 properties may be used to capture some  
 215 aspect of the canopy either for (empirical)  
 216 correlation with some more desirable vari-  
 217 able, or for parameterizing more complex  
 218 models. Examples include vegetation indices  
 219 such as the normalized difference vegetation  
 220 index (NDVI) and variants, which have been  
 221 widely and successfully used to provide sur-  
 222rogate indicators of canopy ‘greenness’  
 223 (Pettorelli et al. 2005). They are attractive  
 224 due to being easy to calculate and apply,  
 225 and they may capture key aspects of vegeta-  
 226 tion ‘well enough’. NDVI for example  
 227 exploits the characteristic high contrast  
 228 between red and near-infrared (NIR) spectral  
 229 reflectance,  $\rho$  of healthy vegetation as  
 230  $NDVI = (\rho_{NIR} - \rho_{RED}) / (\rho_{NIR} + \rho_{RED})$ . Such  
 231 indices are clearly useful for capturing par-  
 232 ticular broad vegetation patterns, ~~either~~  
 233 in themselves e.g. as indicators of vegetation  
 234 response to climate, disturbance, insect or  
 235 fire damage, malaria risk etc. (Pettorelli  
 236 et al. 2005, 2013; Pfeifer et al. 2012). Vege-  
 237 tation indices can also be used as surrogates  
 238 for empirically-related variables such as leaf  
 239 area index (LAI), the (unitless) one sided  
 240

t.1 *Table 11.1.* List of properties of interest to terrestrial ecosystem studies that can be derived from EO data, categorised broadly by their requirement for additional information and assumptions beyond a direct measurement

t.2	'Directness'	Measurement (units)	Key additional assumptions
t.3	Direct	Top-of-atmosphere at-sensor radiance ( $\text{W m}^{-2} \text{sr}^{-1} \mu\text{m}^{-1}$ ) from reflectance (optical), emittance (passive microwave/thermal), backscatter (RADAR); canopy fluorescence (arbitrary units). Distance from sensor to target i.e. canopy and surface height (m) e.g. from lidar	Calibrated sensor response, geolocated instantaneous field of view (IFOV)  Accurate time-of-flight of active (generated) signal (pulse), known pulse characteristics and position of sensor in 3D space.
t.4	High	Top-of-canopy (surface) radiance ( $\text{W m}^{-2} \text{sr}^{-1} \mu\text{m}^{-1}$ )	Known atmospheric path radiance (via models and/or ancillary data)
t.5		Albedo (unitless)	Known incoming radiation distribution in terms of angular and direct-to-diffuse ratio i.e. function of atmosphere; integrable model of surface angular reflectance distribution
t.6	Medium	Surface temperature (K)	Well-calibrated sensor; surface emissivity
t.7		Canopy structural properties: Leaf area index (LAI, unitless); canopy cover (unitless %); canopy gap fraction (unitless)	Model relating scattered radiation to structural parameters, assume a degree of clumping/Inversion must be tractable and not ill-posed.
t.8		Canopy radiometric properties: fraction of photosynthetically active radiation, fAPAR (unitless); canopy-average biochemical constituents (chlorophyll, water, N and dry matter, mass per unit specific leaf area i.e. $\text{g m}^{-2}$ )	Model relating radiation scattered within and from the canopy to radiometric parameter. Inversion must be tractable and not ill-posed.
t.9		Leaf radiometric properties: biochemical constituents (chlorophyll, water, N and dry matter, mass per unit specific leaf area i.e. $\text{g m}^{-2}$ )	Model relating radiation scattered within and from the leaf. Often embedded into canopy-level model.
t.10		Standing biomass ( $\text{kg C m}^{-2}$ )	Empirical allometric model relating height to biomass (via time-of-flight from lidar, or interferometric RADAR); requires woody biomass to total carbon ratio.
t.11		Fire radiative power (FRP, $\text{W m}^{-2} \mu\text{m}^{-1}$ ) and energy (FRE) ( $\text{J m}^{-2}$ )	FRP requires model relating observed temperature to surface emissivity; FRE requires integration of FRE over time.
t.12		Burned area (ha)	Model of surface bidirectional reflectance distribution function (BRDF) allowing prediction of reflectance and detection of change.
t.13	Low	Standing biomass ( $\text{kg C m}^{-2}$ ) from scattering	Model of reflectance (optical) or backscatter (RADAR) related to biomass; assumption of leaf to wood ratio in canopy and wood density conversion factor;
t.14		Photosynthetic rate ( $\mu\text{mol m}^{-2} \text{s}^{-1}$ )	Model relating leaf absorption or fluorescence, to measured signal
t.15		Gross primary productivity, GPP ( $\text{kg C m}^{-2} \text{h}^{-1}$ )	Incoming radiation, fAPAR, model relating intercepted radiation to gross productivity; ancillary information on biome type, climate (T, P)
t.16		Net primary productivity, NPP ( $\text{kg C m}^{-2} \text{h}^{-1}$ )	GPP, autotrophic respiration losses (measured or modelled)
t.17		Net ecosystem productivity, NEP ( $\text{kg C m}^{-2} \text{h}^{-1}$ )	NPP, heterotrophic respiration losses (measured or modelled)
t.18			

(continued)

t.20 *Table 11.1.* (continued)

t.21	'Directness'	Measurement (units)	Key additional assumptions
t.19		Net ecosystem exchange, NEE ( $\text{kg C m}^{-2} \text{h}^{-1}$ )	NEP, losses due to disturbance (fire, harvest, predation, etc)
t.20		Land cover ( $\text{km}^{-2}$ ), Land use/land use change (LULUC, $\text{km}^{-2}$ )	Unique mapping of vegetation types (or biome) and other spectrally identifiable cover types to land cover classes; LULUC requires mapping between biome/land cover and land use.
t.21	Ambiguous/surrogate	NDVI (and other empirical spectral indices); 'greenness'; phenology.	Land cover or biome type; spectral; definition of 'greenness' – usually some arbitrary translation of a spectral index to vegetation 'vigour' or state; phenology requires definition of canopy timing, as a function of an EO-derived variable, typically NDVI or LAI.

t.22 Key assumptions required to move from more to less direct measurements are outlined. The list is not intended to be exhaustive, and 'directness' is somewhat subjective.

241 leaf area per unit ground area, fraction of  
 242 absorbed photosynthetically active radiation  
 243 ( $f_{APAR}$ ) and hence productivity (Myneni  
 244 et al. 1997a; Angert et al. 2005). However,  
 245 simplicity comes at the cost of ecological  
 246 meaning (i.e. direct causality) and requi  
 247 ment for site- or biome-specific calibrati  
 248 Other more general limitations of vegetation  
 249 indices are the lack of sensitivity with  
 250 increasing LAI, saturating at values of 4–5,  
 251 and sensitivity to background effects (soil,  
 252 haze etc.). Care is also needed when  
 253 compositing vegetation indices over time to  
 254 account for variations in view and sun angles  
 255 in the reflectance observations from which  
 256 the vegetation indices are derived. These  
 257 limitations, particularly saturation, are not  
 258 soluble through taking a particular calibra-  
 259 tion approach.

260 The difficulty of interpreting vegetation  
 261 indices has been seen in the debate over  
 262 unexpected trends in Amazonian green-up  
 263 observed during the severe 2005 drought  
 264 (Saleska et al. 2007; Samanta et al. 2010).  
 265 Subsequent to this, work relating carefully  
 266 re-processed estimates of enhanced vegeta-  
 267 tion index (EVI, another empirical spectral  
 268 index) to ground-based measures of produc-  
 269 tivity, water availability and other ecological  
 270 variables suggested that apparent discre-  
 271 pancies may be due to leaf flushing being  
 272 mistaken for changes in LAI and productiv-  
 273 ity (Brando et al. 2010). This debate was  
 274 rejoined by recent re-analysis of the satellite  
 275 data, including detailed consideration of

276 vegetation structure and satellite-sun geome-  
 277 try (Morton et al. 2014). This approach  
 278 accounts for the apparent 'observed' green-  
 279 up, whilst also ruling out the leaf-flushing  
 280 hypothesis. Crucially, this re-analysis was car-  
 281 ried out on the original satellite spectral reflec-  
 282 tance data, rather than the spectral indices  
 283 derived from those data from which the origi-  
 284 nal 2005 green-up conclusions were drawn.

285 This debate perhaps illustrates the diffi-  
 286 culty of trying to explain variations in empiri-  
 287 cal spectral indices that can be functions of  
 288 complex, often mutually compensating bio-  
 289 physical processes. Verstraete et al. (1996)  
 290 sum up this difficulty by noting that any  
 291 number of empirical functions relating a  
 292 parameter of interest  $Y$  to observations  $Z$   
 293 of the form  $Y = g(Z)$  may be derived. How-  
 294 ever, these relationships effectively assume  
 295 that the variable of interest is the main  
 296 controlling factor of the observations  $Z$  to  
 297 the (near) exclusion of all other factors.  
 298 Since the same vegetation index is often  
 299 used to derive different  $g(Z)$  for different  
 300 applications, the information contained in  $g$   
 301 ( $Z$ ) must be the same, regardless of how the  
 302 vegetation index is interpreted. This is rarely  
 303 acknowledged in practice.

304 The problem of ascribing direct meaning  
 305 to surrogate variables makes them hard  
 306 (or even impossible) to validate. For example  
 307 'greenness' has been used to imply amount  
 308 (Myneni et al. 1997a), productiv  
 309 (degree of stress) and phenology (Petto  
 310 (2013). This latter term is also ambiguous;



311 although it implies seasonality, this can be  
 312 defined to encapsulate a number of differ-  
 313 ent, related things: bud break, leaf emer-  
 314 gence, onset of photosynthesis and growth,  
 315 start of flowering, seasonal LAI profile,  
 316 onset of senescence, leaf drop, growing sea-  
 317 son length etc. A further complication is  
 318 that ecological models that describe plant  
 319 seasonality typically use some integrated  
 320 estimate of time such as growing degree  
 321 days (number of days over a base threshold,  
 322  $T_t$  multiplied by the excess temperature  
 323  $T-T_t$ ). Recent work by Richardson et al.  
 324 (2012) has shown that different model  
 325 representations of phenology tend to intro-  
 326 duce overestimates of canopy productivity  
 327 during spring greenup by 13 %, and during  
 328 autumn senescence by 8 % of total annual  
 329 productivity. This problem was exacerbated  
 330 by the tendency of individual models to  
 331 compensate for over-estimates during tran-  
 332 sition periods by under-prediction of sum-  
 333 mer peak productivity. As a result,  
 334 Richardson et al. (2012) conclude that cur-  
 335 rent model uncertainties preclude reliable  
 336 prediction of future phenological response  
 337 to climate change.

338 The difference between the ways ecologi-  
 339 cal models treat vegetation amount and state  
 340 and how these properties can be derived  
 341 from EO is a key reason for differences  
 342 between models and observations: both  
 343 representations may be internally consistent,  
 344 but inconsistent with each other (of course,  
 345 either or both may be wrong as well!). Lastly,  
 346 even when empirically-derived properties  
 347 appear to correlate well with characteristics  
 348 we wish to measure, we do not know how the  
 349 residual unexplained variance arises, or if it  
 350 is important. For a more detailed discussion  
 351 I refer to Pfeifer et al. (2015) who review a  
 352 range of ecologically-relevant biophysical  
 353 properties available from EO, as well as  
 354 some of the issues in moving from direct to  
 355 more indirect products.

356 Perhaps most importantly then, for under-  
 357 standing and interpreting EO-derived  
 358 measurements of canopy state and function,  
 359 we require physically-based models of radi-  
 360 ation interaction with the canopy. Below, I  
 361 provide a statement of this problem, lay out

362 some of approaches to solving it, and 362  
 363 describe how these approaches are used to 363  
 364 exploit the EO signal for remote sensing 364  
 365 studies of vegetation. Advances in comput- 365  
 366 ing power have meant that highly-detailed 366  
 367 modelling approaches which were previ- 367  
 368 ously impractical have become increasingly 368  
 369 attractive. A good example of this is how 369  
 370 photo-realistic 3D modelling techniques 370  
 371 developed by the computer graphics commu- 371  
 372 nity for movie-making and visualisation, 372  
 373 have been co-opted for modelling vegeta- 373  
 374 tion for scientific applications (Disney et al. 374  
 375 2006; Widlowski et al. 2006). This in turn 375  
 376 has led to improved parameter estimation 376  
 377 schemes (Disney et al. 2011), allowed 377  
 378 assessed of uncertainty, and provided test 378  
 379 and benchmark tools for simpler modelling 379  
 380 approaches (Widlowski et al. 2008, 2013). 380  
 381 Rapid increases in computation speed have 381  
 382 also led to changes in the way information 382  
 383 can be derived from very large (GB to TBs) 383  
 384 satellite datasets. This is almost always a 384  
 385 balance between requirements for speed/effi- 385  
 386 ciency, and accuracy or physical realism. 386  
 387 Increasingly, statistical tools such as Monte 387  
 388 Carlo and Bayesian methods, which had 388  
 389 been too slow for these applications, can be 389  
 390 employed (Sivia and Skilling 2006). 390

391 I discuss some of these developments in 391  
 392 canopy modelling in more detail below, 392  
 393 before moving on to discussing recent 393  
 394 developments in model-data fusion that are 394  
 395 pushing the limitations of both, and the 395  
 396 advent of new observations that may provide 396  
 397 information more directly-related to the 397  
 398 problems at hand. I embark on this descrip- 398  
 399 tion with a quote that encapsulates the diffi- 399  
 400 culty that can arise in trying to reconcile 400  
 401 models (hypotheses) and measurements, in 401  
 402 part due to the different scientific drivers and 402  
 403 assumptions that underlie them; this is par- 403  
 404 ticularly apposite in remote sensing, where 404  
 405 the two are so intimately intertwined. 405

406 A hypothesis is clear, desirable and positive, but is 406  
 407 believed by no one but the person who created 407  
 408 it. Experimental findings, on the other hand, are 408  
 409 messy, inexact things which are already believed 409  
 410 by everyone except the person who did the work 410  
 411 (Harlow Shapley (1885–1972), *Through Rugged*  
 412 *Ways to the Stars*, 1969). 412

## II. Radiative Transfer in Vegetation: The Problem and Some Solutions

We are rarely interested in the most direct EO measurement we can make i.e. in top-of-atmosphere radiance resulting from photons incident on the surface that are scattered in some way back towards the sensor (Pfeifer et al. 2012). In order to relate the above-atmospheric signal to the structural (amount, arrangement) and biochemical (absorbing species and concentrations) properties of the canopy we need a physically realistic description of the radiation scattering properties of the canopy. This in turn requires understanding of the canopy radiative transfer (RT) regime from the leaf level, across scales to shoot and crown levels, and finally to the whole canopy.

### A. Statement of the Radiative Transfer Problem

RT models have been used extensively since the 1960s to model scattering from canopies at optical wavelengths (Ross 1981; Myneni et al. 1989). The models consider energy balance across an elemental volume in terms of the energy arriving into the volume (either energy incident in the propagation direction, or energy that is scattered from other directions) and energy losses from the volume (either scattering out of the propagation direction, or absorption losses). Across optical wavelengths (visible, NIR and shortwave infrared (SWIR) regions of 400–2500 nm) a scalar radiative transfer equation is used. At RADAR wavelengths (cm to m), a slightly different approach is required, incorporating a vector of intensities to allow consideration of polarization (controlled by the sensor design). In this case orthogonal polarizations are coupled so radiative transfer equations must take this into account in a vector solution. Here I focus on radiative transfer in the optical domain, due to the particular relevance to canopy activity.

A widely-applied approach to describing radiation transport in vegetation has been via

the so-called turbid medium approximation (Ross 1981; Myneni et al. 1989; Liang 2004). This considers the canopy as a plane parallel homogeneous medium of infinitesimal, oriented scattering elements, suspended over a scattering (soil) background – a ‘green gas’. In this case, mutual shading can be ignored (the ‘far field’ approximation) and the radiance field resulting from single and multiple scattered photons can be described by considering the conservation of energy within a canopy layer, and specifying the sources of radiation external to that layer (boundary conditions). The result is an integro-differential equation describing the change in intensity  $I$  along a viewing direction  $\Omega(\theta_v, \varphi_v)$  due to: (i) interactions causing radiation to be scattered out of the illumination direction  $\Omega'(\theta_i, \varphi_i)$  (sink term); and (ii) interactions causing radiation to be scattered from other directions into the viewing direction  $\Omega(\theta_v, \varphi_v)$  (source term), where  $\theta_{i,v}$  and  $\varphi_{i,v}$  are the illumination and view zenith and azimuth angles respectively. This system is shown schematically in Fig. 11.1.

The far-field approximation allows us to ignore polarization, frequency shifting interactions and emission, in which case the upward and downward energy fluxes within the canopy are described by the (1D) scalar radiative transfer equation. For a plane parallel medium (air) embedded with a low density of small scattering objects the radiative transfer equation is composed of two terms, the (negative) extinction term with depth  $z$  that is determined by the path length through the canopy and the extinction along this path, and the source term due to multiple scattering from all directions within an elemental volume in the canopy into direction  $\Omega$  by the objects in the volume. Thus,

$$\mu \frac{\partial I(z, \Omega)}{\partial z} = -\kappa_c I(z, \Omega) + J_s(z, \Omega) \quad (11.2)$$

where  $\partial I(z, \Omega)/\partial z$  is the steady-state radiance distribution function and  $\mu$  is the cosine of the (illumination) direction vector  $\Omega'$  with the local normal i.e. the viewing zenith

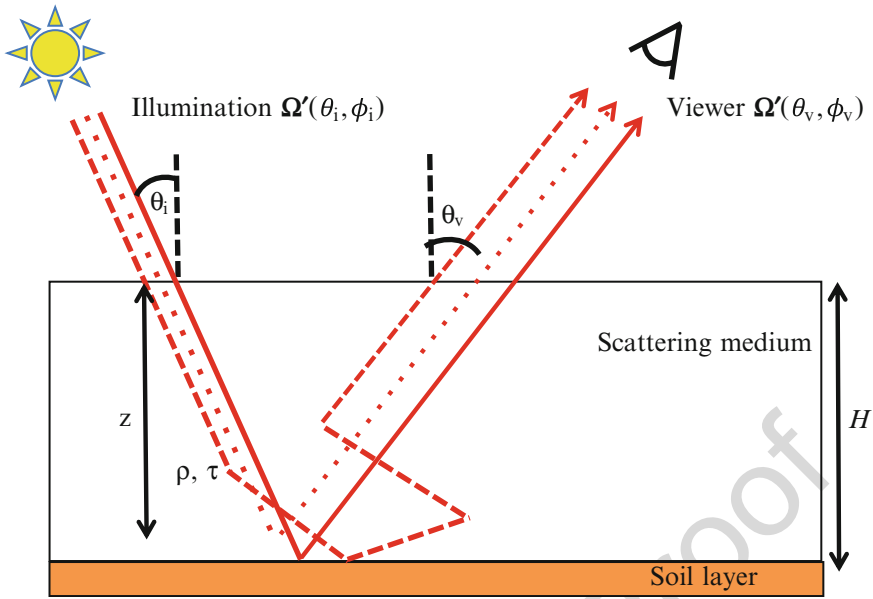


Fig. 11.1. Schematic illustration of radiation incident on a plane parallel homogeneous medium (solid line), at a zenith angle  $\theta_i$ ; azimuth angle  $\phi_i$  from the surface normal and penetrating to a depth  $z$  (marked by dashed line). In this example incoming radiation either passes through uncollided to the lower boundary, and back up (solid line); is scattered once at depth  $z$  by reflectance (dotted line); or is scattered multiple times via reflectance and/or transmittance, including the canopy lower boundary (at  $z = -H$ ) before escaping in the viewing direction (dashed line)

503 angle,  $\theta_i$  used to account for path length  
 504 through the canopy. The extinction term is  
 505 given as the product of  $\kappa_e$ , the volume extinction  
 506 coefficient, and  $I(z, \Omega)$ , the specific  
 507 energy intensity in direction  $\Omega$  at depth  
 508  $z$  within a horizontal plane-parallel canopy  
 509 of total height  $H$  ( $0 < z < H$ ). The source  
 510 term,  $J_s(z, \Omega')$ , is defined as

$$J_s(z, \Omega') = \int_{4\pi} P(z, \Omega' \rightarrow \Omega) I(z, \Omega) d\Omega' \quad (11.3)$$

511 where  $P(z, \Omega' \rightarrow \Omega)$  is the volume scatter-  
 512 ing phase function. This defines the (angu-  
 513 lar) probability of a photon at depth  $z$  in the  
 514 canopy being scattered from the illumination  
 515 direction  $\Omega'$  through a solid angle  $d\Omega'$  into to  
 516 the viewing direction,  $\Omega$ , integrated over the  
 517 unit viewing hemisphere. This term depends  
 518 on the size and orientation of scatterers  
 519 within the canopy (see below).

When this description is extended to 3D, 520  
 i.e. the canopy can vary in density in vertical 521  
 and horizontal directions, the illumination 522  
 and viewing vectors are functions of both 523  
 the zenith and azimuth angles  $\theta_{i,v}$  and  $\phi_{i,v}$  524  
 i.e.  $\Omega'(\theta_i, \phi_i)$  and  $\Omega(\theta_v, \phi_v)$  respectively. 525

A full description of radiative transfer 526  
 should include the corresponding emission 527  
 source term  $J_s(z, \Omega')$  for wavelengths where 528  
 this might be significant e.g. for passive 529  
 microwave (thermal) emissions from objects 530  
 at  $\sim 300$  K ( $\sim 8\text{--}20 \mu\text{m}$ ). In this case each 531  
 object within the medium may need to be 532  
 considered as an emission source in its own 533  
 right. However, for optical and RADAR 534  
 wavelengths, the emission source term is 535  
 effectively zero. 536

Solving Eq. 11.2 requires defining  $\kappa_e$  in 537  
 terms of canopy biophysical properties, and 538  
 considering a particular viewing direction 539  
 $\Omega'$ , for given boundary conditions. In using 540  
 Eq. 11.2 to model canopy scattering for 541  
 remote sensing applications, we wish to 542  
 phrase the scattered radiation as an intrinsic 543

544 property of the canopy, rather than as a func-  
 545 tion of incident intensity. This permits compar-  
 546 ison of measurements made under  
 547 differing illumination intensities. At optical  
 548 wavelengths this fundamental intrinsic scatter-  
 549 ing quantity wavelengths is known as the  
 550 Bidirectional Reflectance Distribution Function  
 551 (BRDF) i.e.:

$$\text{BRDF}(\Omega, p, \Omega', p'; \lambda) = \frac{dI_r(\Omega, p', F; \lambda)}{dE_i(\Omega', p; \lambda)} \quad (11.4)$$

552 where  $p$  and  $p'$  are the polarization of the  
 553 received/transmitted wave;  $E_i$  is the  
 554 downwelling irradiance on the surface  
 555 ( $\text{W m}^{-2}$ ); and  $I_r$  is the upwelling (reflected)  
 556 radiance ( $\text{W m}^{-2} \text{sr}^{-1}$ ). The BRDF of an  
 557 ideal diffuse (Lambertian) surface is  $1/\pi$   
 558 (for an unpolarized reflector) and is independ-  
 559 ent of viewing and illumination angles. As  
 560 defined, BRDF is an infinitesimal quantity  
 561 (with respect to solid angle and wavelength),  
 562 so although it can be modelled, it is not a  
 563 measurable quantity in this form. In practice,  
 564 we consider the Bidirectional Reflectance  
 565 Factor (BRF)  $\rho_c(\Omega, \Omega')$ , defined as the ratio  
 566 of radiance leaving the surface around  
 567 viewing direction  $\Omega$ ,  $I(\Omega)$  due to irradiance  
 568  $E(\Omega')$ , to the radiance on a flat totally reflect-  
 569 ive Lambertian surface under the same  
 570 illumination conditions i.e.

$$\begin{aligned} \rho_c(\Omega, \Omega') &= \frac{E(\Omega') \text{BRDF}(\Omega, \Omega')}{E(\Omega')(1/\pi)} \\ &= \pi \text{BRDF}(\Omega, \Omega') \end{aligned} \quad (11.5)$$

571 for an equivalent infinitesimal solid angle  
 572 definition. As the BRF is defined as the  
 573 ratio of two radiances, it is a directly meas-  
 574 urable quantity and allows for model  
 575 predictions to be compared with measure-  
 576 ments, albeit over instrument finite solid  
 577 angles (and of course wavelength intervals).  
 578 Detailed definitions of reflectance nomencla-  
 579 ture are given by Nicodemus et al. (1977)  
 580 and Schaepman-Strub et al. (2006).

## B. Solving the Radiative Transfer Problem for Explicit Canopy Structure 581 582

To solve the radiative transfer problem for realistic canopies, we need to consider how vegetation structure can be expressed in terms of the equations above, using assumptions that permit physically realistic solutions. Various solutions for the radiative transfer equation have been developed in a range of subjects including astrophysics, particle physics and neutron transport (Chandrasekhar 1960). Most importantly, once we have a solution of Eq. 11.2, if it can be inverted in terms of the canopy parameters it contains, we can then estimate distributions of these parameters from EO measurements of  $\rho_c(\Omega, \Omega')$  in the standard inverse problem sense (Twomey 1977; Verstraete et al. 1996; Tarantola 2005). Forward and inverse approaches to canopy modelling have been reviewed in detail by Asrar (1989), Goel (1989), Goel and Thompson (2000) and more recently by Liang (2004), among others, and I provide a brief overview here.

Solving the forward radiative transfer problem either requires empirical parameterisations or physically-based approximations of canopy properties including leaf size, angle distribution and 1D or 3D arrangement. Some applications do not require a physically-meaningful interpretation of model parameters, only a reasonable prediction of  $\rho_c(\Omega, \Omega')$ . For example, many remote sensing applications require comparing observations made over time (and/or using wide-angle sensors). These observations are typically acquired at different view and/or illumination angles, so variations in reflectance caused by these varying view and sun angles (i.e. BRDF effects) must be accounted for, otherwise they may be interpreted as surface changes. A widely-used approach is to fit a simple empirical (or semi-empirical) model of BRDF to observations, and use the resulting (inverted) model parameters to interpolate (or normalize) observations to a fixed view and illumination configuration. The simple nature of semi-empirical

BRDF models means they can be inverted rapidly, making them suitable for rapid, large-scale applications. Observations from the NASA MODIS and MISR sensors employ variants of this approach to account for sensor and sun angle variations (Pinty et al. 1989; Wanner et al. 1997).

Physically-based models of BRDF are required to represent three specific processes:

1. Coherent superposition of scattered incident radiation. This is dependent on the mean free path between scattering events within the canopy being of the order of the wavelength of the incident radiation. Coherence is generally ignored for vegetation, but is important for soils.
2. Scattering effects resulting from the arrangement of objects on the surface, i.e. specular reflectance, and reflectance variations caused by geometric-optic shadowing assuming parallel rays of incident radiation.
3. Volume (diffuse) scattering of aggregated canopy elements. This is particularly important for dense vegetation and is modelled using radiative transfer methods as outlined above. As higher orders of photon scattering are considered, the interactions become increasingly random in direction, and the volume scattering component tends to become isotropic.

To solve Eq. 11.2, approximations regarding the leaf scattering properties are often made (e.g. Myneni et al. 1989). Other approaches attempt to include modifications for observed features that occur due to the fact that real vegetation canopies are not turbid media and leaves, branches etc. have finite sizes. The most obvious of these features is the so-called ‘hotspot’, an increase in reflectance seen when  $\Omega$  and  $\Omega'$  are near-coincident, that arises due to shadowing in the scene being at a minimum (Nilson and Kuusk 1989). An example of this phenomenon is shown in Fig. 11.2 As an example of the importance of considering canopy structure on the EO signal, Morton et al. (2014) demonstrate that the apparent

Amazon ‘greenup’ observed in 2005 can be explained almost entirely as a BRDF effect: most observations made in October in this location are in the hotspot i.e. the observed increase in reflectance is an angular effect.

Perhaps the most difficult problem in solving Eq. 11.2 is that of modelling the source term,  $J_s(z, \Omega)$  as this requires keeping a ‘scattering history’ of each photon from one interaction to the next. This problem is essentially insoluble analytically (Knyazikhin et al. 1992), but numerical approximations can be made or computer simulation models can be used (see below). It is also necessary to define the boundary conditions in the case of a canopy illuminated from above. At the top of the canopy the incident irradiation can be considered as diffuse and direct components of solar irradiation. In addition, some radiation arriving at the base of the canopy re-radiates isotropically back up through the canopy effectively creating a source function at the lower canopy boundary. Modified forms of Eq. 11.2 have been widely used to model canopy reflectance for a range of applications. Further approximations and simplifications have been applied for specific types of canopy, such as row crops or particular tree crown shapes. In these cases, simplifying approximations can be made regarding canopy structure, in particular the vertical and horizontal arrangement of leaves and their angular orientations (distribution functions). Various approaches are summarised by Goel (1988), Strahler (1996), Liang (2004) and Lewis (2007, from <http://www2.geog.ucl.ac.uk/~plewis/CEGEG065/rtTheoryPt1v1.pdf> and <http://www2.geog.ucl.ac.uk/~plewis/CEGEG065/rtTheoryPt2v7-1.pdf>).

Separation of canopy fluxes into uncollided and collided intensities of various orders (Kubelka and Munk 1931; Suits 1972; Hapke 1981) has often been employed in order to simplify the radiative transfer approach (Norman et al. 1971; Myneni et al. 1990; Verstraete et al. 1990). The simplest two-stream approach decomposes multiple scattering into upward and downward diffuse fluxes. This can be



*Fig. 11.2.* Illustration of the canopy hotspot effect. The image was captured with the sun directly behind the camera (see shadow of aircraft in the centre) and the scene is brightest at the centre, darkening radially outwards due to shadows becoming increasingly visible (author's own, taken over temperate rainforest canopy, Fraser Island, Queensland, Australia)

728 elaborated in e.g. a four-stream approxima- 751  
 729 tion into fluxes resulting from reflectance 752  
 730 and transmittance interactions respectively. 753  
 731 The discrete properties of the canopy, those 754  
 732 related to the size and distribution of 755  
 733 scatterers, tend to impact only the first few 756  
 734 orders of scattering and these features tend to 757  
 735 become 'smeared out' by higher order multiple 758  
 736 scattering interactions. Dividing the 759  
 737 radiation field into collided and uncollided 760  
 738 intensities as opposed to following a standard 761  
 739 radiative transfer treatment may preserve 762  
 740 these features. 763

741 As the canopy becomes denser, mutual 764  
 742 shading of scattering elements cannot be 765  
 743 ignored. It also becomes increasingly difficult 766  
 744 to justify the use of convenient values 767  
 745 for the scattering phase function i.e. the 768  
 746 assumptions that leaf normals are randomly 769  
 747 oriented and azimuthally invariant in defining 770  
 748 leaf normal distribution and leaf projection 771  
 749 function. This is clearly partially or 772  
 750 wholly violated for a number of canopies, 773

751 particularly for row-oriented agricultural 752  
 753 crops. Various approaches have been proposed 754  
 755 to overcome this. However, Knyazikhin et al. (1998) 756  
 757 have shown that accounting for the discrete nature of 758  
 759 vegetation within a (continuous) radiative transfer 760  
 761 description leads to an apparent paradox: the more 762  
 763 accurate the representation of canopy geometry, the 764  
 765 less accurate the resulting description of radiative 766  
 767 transfer and photosynthesis in the canopy is likely to 768  
 769 be. This arises because of the discrepancy between 769  
 770 the assumption of a continuous homogeneous scattering 770  
 771 medium underpinning the radiative transfer approach, 771  
 772 and the macroscopic effects of 3D leaf and branch size 772  
 773 and distribution. Knyazikhin et al. (1998) point 773  
 774 out that the radiative transfer approach assumes that 774  
 775 the number of foliage elements in an elementary volume 775  
 776 is proportional to this volume (encapsulated in the 776  
 777 leaf area density), but the larger leaves become are 777  
 778 in relation to the volume, the less this 778

774 assumption holds. The impact of this depar-  
775 ture therefore decreases as we look at larger  
776 scales/volumes.

777 One of the most powerful approximations  
778 used in radiative transfer modelling is to  
779 concentrate on single scattering interactions  
780 only. These are in many cases the dominant  
781 component of canopy scattering (Myneni  
782 and Ross 1990), particularly at visible  
783 wavelengths. Considering single scattering  
784 interactions within a turbid medium, the  
785 radiation intensity in the incident direction  
786  $\Omega'$ , at a depth  $z$  within the canopy can be  
787 described using Beer's (Beer-Bouguer-  
788 Lambert's) Law (Monsi and Saeki 1953)  
789 as follows

$$I(z, \Omega') = I(0, \Omega') e^{-\left(\frac{L(z)G(\Omega')}{\mu'}\right)} \quad (11.6)$$

790 where  $I(0, \Omega')$  is the incident irradiance at  
791 the top of the canopy;  $L(z)$  is the cumulative  
792 leaf area index (LAI) in the canopy at depth  
793  $z$  ( $\text{m}^2 \text{m}^{-2}$ );  $G(\Omega')$  is the leaf projection  
794 function i.e. the fraction of leaf area  
795 projected in the illumination direction  $\Omega'$ ;  
796  $\mu' = \cos(\theta_i)$ .

797 The exponent in Eq. 11.6 is effectively the  
798 extinction coefficient  $\kappa_e$  i.e. a measure of the  
799 rate of attenuation of radiation in the canopy,  
800 and is a function of two things: (i) the  
801 amount of material along the path i.e.  
802 the domain-averaged optical thickness of  
803 the canopy layer  $LAI$ ; and (ii) the volume  
804 absorption and scattering properties of  
805 the media i.e. loss due to absorption by the  
806 particles (leaves) and scattering by the  
807 particles away from the direction of propa-  
808 gation (Fung 1994). The term  $L(z)$  is better  
809 defined as  $u_1(z)$ , the canopy leaf area density  
810 i.e. the vertical distribution of one-sided leaf  
811 area per unit canopy volume ( $\text{m}^2$  of leaf area  
812 per  $\text{m}^3$  of canopy volume). We will see later  
813 in Section III that this exponent implicitly  
814 encapsulates the fact that canopies are not  
815 homogeneous but are actually clumped at  
816 multiple scales from leaf to branch to  
817 crown. Assuming a constant leaf area of  $A_l$ ,  
818 and given a leaf number density of  $N_v(z)$

(number of leaves per unit volume,  $\text{m}^{-3}$ ), 819  
then 820

$$u_1(z) = N_v(z)A_l \quad (11.7)$$

The integral of  $u_1(z)$  over the canopy depth, 821  
 $H$ , gives the LAI i.e. 822

$$\text{LAI} = \int_{z=0}^{z=H} u_1(z) dz \quad (11.8)$$

In practice,  $u_1(z)$  may vary from top to bot- 823  
tom of a canopy, with more material perhaps 824  
in the upper parts than in the lower parts. As 825  
a result,  $L(z)$  can be modelled in various 826  
ways in a radiative transfer scheme, but the 827  
simplest is to assume it is constant with 828  
canopy height  $H$  i.e.  $u_1 = \text{LAI}/H$ . 829

The term  $G(\Omega')$  in Eq. 11.6 is the projec- 830  
tion of a unit area of foliage on a plane 831  
perpendicular to the illumination direction 832  
 $\Omega'$ . By extension,  $G_1(\Omega)$  is the leaf projection 833  
function in the viewing direction  $\Omega$ , aver- 834  
aged over elements of all orientations and is 835  
a (unitless) canopy-average representation of 836  
the effective leaf area encountered by a pho- 837  
ton travelling in a direction  $\Omega$  within the 838  
canopy.  $G_1(\Omega)$  is defined as 839

$$G_1(\Omega) = \frac{1}{2\pi} \int_{2\pi+} g_1(\Omega_1) |\Omega \cdot \Omega_1| d\Omega_1 \quad (11.9)$$

where  $g_1(z, \Omega_1)$  is the angular distribution of 840  
leaf normal vectors, known as the leaf angle 841  
distribution (LAD) and is defined so that its 842  
integral over the upper hemisphere is 1 i.e. 843

$$\int_{2\pi+} g(\Omega_1) d\Omega_1 = 1 \quad (11.10)$$

A wide range of choices for models of 844  
 $g_1(z, \Omega_1)$  have been proposed (Ross 1981; 845  
Goel and Strebel 1984). A typical assump- 846  
tion is that leaf azimuth angles are independ- 847  
ent of azimuth i.e.  $g_1(\Omega_1) = g_1(\theta_1)h_1(\phi_1)$  848  
where  $h_1(\phi_1)$  is the azimuthal dependence 849  
and can be specified separately as 850

851  $(1/2\pi) \int_{\phi_1=0}^{\phi_1=2\pi} h_1(\phi_1) d\phi_1 = 1$ . If the azimuthal  
 852 distribution is assumed to be uniform  
 853 (i.e. random) then  $h_1(\phi_1) = 1$  and this allows  
 854 for expression of  $g_1(z, \Omega_1)$  as a function of  $\theta_1$   
 855 only and  $\int_{\theta_1=0}^{\theta_1=\pi/2} g_1(\theta_1) \sin \theta_1 d\theta_1 = 1$ . While

856 these assumptions make the formulation of  
 857  $g_1(\theta_1)$  easier, it is known that many canopies  
 858 depart from them particularly in the case of  
 859 strongly-row oriented canopies (crops), or  
 860 due to environmental factors such as wind  
 861 and water stress (e.g. wilting) and heliotropism.  
 862 Tree crowns may also have particular  
 863 azimuthal arrangement due to branching  
 864 structure, particularly in conifers. Jones and  
 865 Vaughan (2010) discuss measured LADs  
 866 and their departures from radiative transfer  
 867 assumptions.

868 Caveats aside, a number of leaf angle  
 869 archetypes (simple analytical expression  
 870 representing particular LADs) have been  
 871 used to model LAD, covering a wide range  
 872 of observed canopy types (Wang et al. 2007).  
 873 These include:

- 874 • planophile – favouring horizontal leaves
- 875 • erectophile – favouring vertical leaves
- 876 • spherical – distributed as if leaves were  
 877 distributed parallel to the surface of a sphere  
 878 and so favouring vertical over horizontal, but  
 879 less than erectophile
- 880 • plagiophile – favouring leaves with angles  
 881 mid-way between erect and flat
- 882 • extremophile – favouring leaves with angles at  
 883 either end of the distribution

884  
 885 An alternative, more general approach  
 886 has been to use ellipsoidal leaf angle  
 887 distributions (Campbell 1986; Flerchinger  
 888 and Yu 2007). These tend to give improved  
 889 solutions for absorption, but at the cost of  
 890 more complex models. Hence large-scale  
 891 remote sensing and Earth system model  
 892 applications strongly favour the simpler

approaches due to the requirements for 893  
 speed. 894

A more flexible alternative to specifying 895  
 archetypes, is to use a parameterisation of 896  
 $g_1(\theta_1)$  which covers the same variation as 897  
 these archetypes. Bunnik (1978) proposed 898  
 a simple four-parameter combination of geo- 899  
 metric functions; Goel and Strebel (1984) 900  
 used a two-parameter Gamma function. The 901  
 Bunnik (1978) model is shown in Eq. 11.11 902  
 (assuming  $g_1(\theta_1)$  is independent of azimuth) 903

$$g(\theta_1) = \frac{2}{\pi} [(a + b \cos(2c\theta_1)) + d \sin \theta_1] \quad (11.11)$$

Examples of the behaviour of the Bunnik 904  
 model are shown Fig. 11.3. The fixed 905  
 archetypes of Ross (1981) agree with these 906  
 parameterisations very closely across all 907  
 angles. The uniform distribution (not shown 908  
 in Fig. 11.3) i.e. randomly-distributed leaf 909  
 normals, is often assumed for simplicity but 910  
 is rarely seen in practice. 911

The turbid medium approximation 912  
 permits a description of canopy scattering 913  
 as a function of a small number of structural 914  
 parameters. Various models have been based 915  
 on the approach outlined above originating 916  
 from the work of Monsi and Saeki (1953). 917  
 The major assumption underpinning Beer's 918  
 Law is that the number of scattering objects 919  
 in a volume of canopy (leaves, stems etc.) 920  
 is proportional to its volume. However, 921  
 Knyazikhin et al. (1998) show that the can- 922  
 opy structure may in some cases be fractal, 923  
 resulting in non-linear relationships between 924  
 canopy volume and the density of scattering 925  
 elements, violating the assumptions of 926  
 Beer's Law. However, the basic formulation 927  
 of Beer's Law can be a useful tool in describ- 928  
 ing single scattering interactions within the 929  
 canopy (Monsi and Saeki 1953). This issue 930  
 of non-random spatial distribution of canopy 931  
 material (clumping) is discussed further 932  
 below. 933

A major drawback of the turbid medium 934  
 approximation is that the size of the scatter- 935  
 ing objects within the canopy is not consid- 936  
 ered. By definition, the canopy is assumed to 937



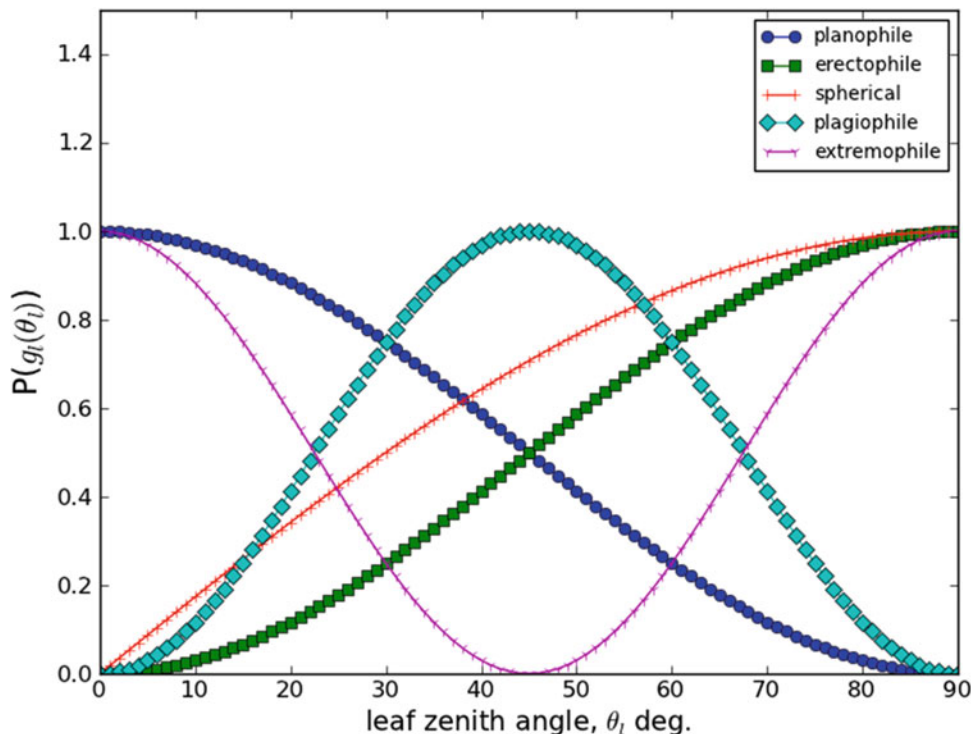


Fig. 11.3. Examples of (normalized) leaf angle distribution functions generated using the Bunnik (1978) four parameter model with parameter value sets: (1, 1, 1, 0), (1, -1, 1, 0), (0, 0, 0, 1), (1, -1, 2, 0) and (1, 1, 2, 0) in legend order

938 be a homogeneous medium of infinitesimal  
 939 scatterers (to satisfy the far-field approxima-  
 940 tion) with mutual shading not permitted.  
 941 Consequently, expressions describing the  
 942 reflected radiation from such a canopy do  
 943 not contain information regarding the size  
 944 of scattering objects. However, certain  
 945 properties of observed canopy scattering  
 946 are directly controlled by the size and orien-  
 947 tation of scattering objects (e.g. Pinty  
 948 et al. 1989). A canopy-level example of this  
 949 impact of finite leaf size is the hotspot effect.  
 950 At the leaf level, the penumbra effect is of  
 951 particular importance to photosynthesis,  
 952 which depends very strongly on the leaf-  
 953 level irradiance. The penumbra effect  
 954 describes the fact that irradiance at the leaf  
 955 is neither wholly direct nor diffuse, but  
 956 somewhere in between, a consequence of  
 957 the finite size of both the solar disk (light  
 958 rays are never perfectly parallel) and the  
 959 leaf (Cescatti and Niinemets 2004). Turbid

medium approximations will not capture 960  
 such features, and if the size of scattering 961  
 objects is to be considered a different 962  
 approach is needed to model the dimensions 963  
 of scattering elements explicitly (Myneni 964  
 et al. 1989). 965

As we can see, solving the radiative trans- 966  
 fer equation in a vegetation canopy is a 967  
 complex problem. Inverting the resulting 968  
 models must generally be performed numeri- 969  
 cally, or using look-up-tables. Additionally, 970  
 the approximations made in order to solve 971  
 Eq. 11.2 result in the model driving param- 972  
 eters being relatively ‘far-removed’ from 973  
 parameters directly representative of phys- 974  
 ical canopy properties. This issue of so-called 975  
 ‘effective parameters’ is critical to applica- 976  
 tions of remote sensing and is discussed fur- 977  
 ther below. First, I look at how radiative 978  
 transfer is considered at the leaf level. Fol- 979  
 lowing this, a relatively new approach to 980  
 radiative transfer modelling is outlined, 981

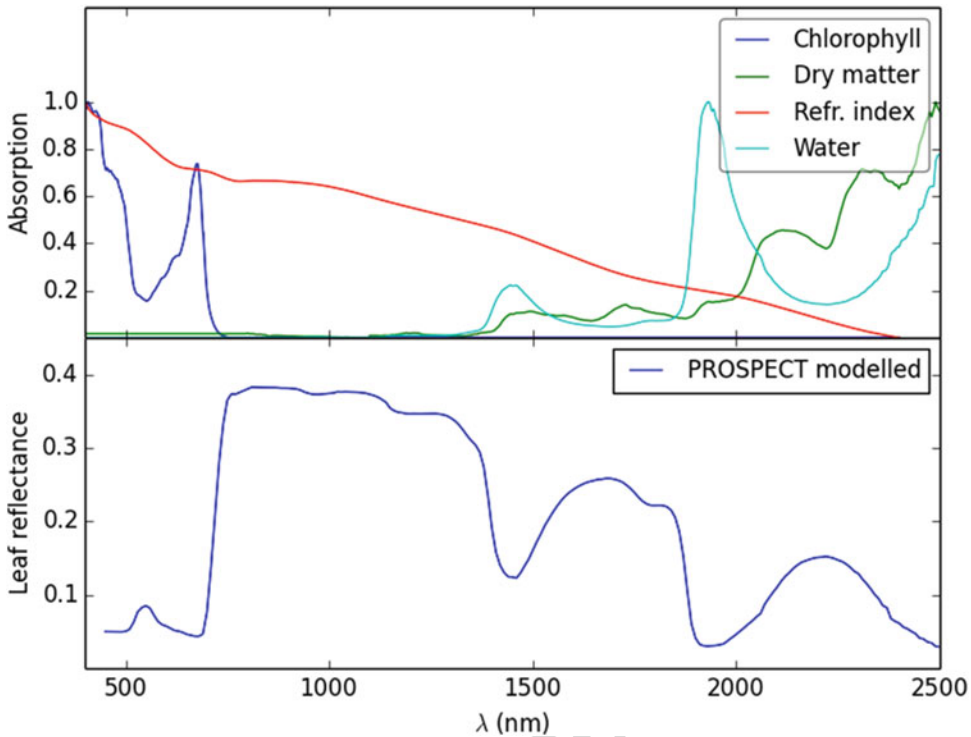


Fig. 11.4. Normalized absorption coefficients used within the PROSPECT model (upper panel) and leaf spectral reflectance modelled by PROSPECT from these absorbing constituents (lower panel)

982 which scales from leaf to canopy, and has  
 983 significant consequences for understanding  
 984 the links between canopy structure and  
 985 biochemistry.

986 *C. Radiation Transfer Within the Leaf*

987 Now we have a description of radiation  
 988 transfer in a canopy, the issue arises of radi-  
 989 ation interactions at the scale of leaves. This  
 990 problem is analogous to the canopy case:  
 991 radiation can penetrate the air/surface inter-  
 992 face depending on the surface properties  
 993 (waxy, smooth etc.) and can either pass  
 994 through air gaps within the leaf unimpeded  
 995 or be scattered, across cell walls into and  
 996 through cells, as well as at the boundaries  
 997 between cells and cell/air. Scattering within  
 998 the leaf will depend on the amount of materi-  
 999 al encountered by a photon (function of  
 1000 leaf thickness, analogous to leaf area density  
 1001 at the canopy level) and the absorption  
 1002 properties of the materials(s), typically the

concentrations of absorbing pigments (chloro- 1003  
 phyll, carotenoids, flavonoids), water and 1004  
 other absorbents such as lignin and cellulose. 1005  
 It is the pigments, and their relationships to 1006  
 leaf/canopy state and nutrient concentrations 1007  
 (particularly leaf N), that are often of interest 1008  
 via remote sensing (Ollinger 2011). 1009

Various approaches to modelling radiative 1010  
 transfer within the leaf have been proposed 1011  
 and Jacquemoud and Ustin (2008) provide 1012  
 an excellent overview. Leaf models require 1013  
 at the very least some description of the 1014  
 refractive index (essentially a structural 1015  
 effect, modifying behaviour at boundaries 1016  
 of scattering materials within the leaf such 1017  
 as cell walls, air and water etc.), and the 1018  
 specific absorption coefficients of absorbing 1019  
 constituents within the leaf. Examples of 1020  
 these properties taken from the widely-used 1021  
 PROSPECT model of Jacquemoud et al. 1022  
 (1996) are given in Fig. 11.4 along with a 1023  
 modelled leaf spectrum for comparison. 1024  
 This illustrates the very specific wavelength 1025

1026 ranges over which the absorption properties  
1027 act: chlorophyll pigment dominates the  
1028 visible; refractive index (leaf structure)  
1029 dominates beyond this into the NIR; water  
1030 and to a lesser extent dry matter (such as  
1031 cellulose and lignin) dominate beyond  
1032 1300 nm. In the UV region, proteins, tannins  
1033 and lignin are important, but these regions  
1034 are rarely used in large-scale remote sensing  
1035 due to the absorption of the solar signal  
1036 by the atmosphere.

1037 Leaf radiative transfer models essentially  
1038 follow one of four broad schemes. The first  
1039 and perhaps simplest approach considers a  
1040 leaf as a semi-transparent plate with plane  
1041 parallel surface, and some surface roughness  
1042 (Allen et al. 1969). Scattering from the leaf  
1043 is calculated as the total sum of successive  
1044 orders of scattering from reflections and  
1045 refractions at the plate boundaries with the  
1046 air. This approach has been generalised to  
1047 consider multiple plane parallel plates by  
1048 decomposing the total upward and down-  
1049 ward fluxes (a two-stream approach) into  
1050 the separate fluxes from each plate (Allen  
1051 et al. 1970). This latter approach is used in  
1052 PROSPECT, perhaps the most widely-used  
1053 leaf radiative transfer model for remote sens-  
1054 ing applications. The model has developed  
1055 over a number of iterations through inclusion  
1056 of more detailed treatment of absorption  
1057 coefficients in particular (Feret et al. 2008).  
1058 PROSPECT has been used to explore the  
1059 impact of biochemistry on leaf reflectance,  
1060 to infer optical properties from remote sens-  
1061 ing measurements, and been coupled to can-  
1062 ope radiative transfer schemes (Jacquemoud  
1063 et al. 2009).

1064 An alternative approach for modelling  
1065 radiative transfer properties of leaves that  
1066 do not conform to the plane parallel approx-  
1067 imation, such as needles, has been to con-  
1068 sider scattering from discrete particles such  
1069 as spheres. The LIBERTY model of Dawson  
1070 et al. (1998) follows this approach, using the  
1071 formulation of Melamed (1963) for scatter-  
1072 ing from suspended powders. Particle size is  
1073 assumed  $\gg \lambda$ , and scattering is again a func-  
1074 tion of successive internal reflections and

refractions, but from within spheres in this  
case, rather than plates.

1075  
1076  
1077 One of the difficulties in developing and  
1078 testing leaf models has been the concomitant  
1079 difficulty of measuring leaf optical proper-  
1080 ties, either in the lab or the field. Measure-  
1081 ment equipment has certainly improved in  
1082 recent years, with the development of porta-  
1083 ble field spectrometers and integrating  
1084 spheres. However, leaf measurements are  
1085 still challenging as they involve handling  
1086 and mounting leaf material without damag-  
1087 ing it, controlling environmental lighting  
1088 conditions, making reference measurements  
1089 etc. Thus the number of high quality leaf  
1090 measurements that can be used for testing  
1091 models, particularly for needles, or non-flat  
1092 leaves is rather small (see for example  
1093 Hosgood et al. 1995).

1094 A range of more general radiative transfer  
1095 modelling approaches have been proposed  
1096 for the particular size problem of leaves.  
1097 One solution of this class is the development  
1098 of Kubelka-Munk theory to provide a 2- or  
1099 4-stream approximation to represent the  
1100 upward and downward fluxes (separated  
1101 into diffuse and direct in the 4-stream case)  
1102 within a single leaf layer, or multiple layers  
1103 (Vargas and Niklasson 1997). This type of  
1104 model has the advantage of allowing analyt-  
1105 ical solutions in certain specific cases. An  
1106 alternative is to solve the radiative transfer  
1107 problem numerically, via Monte Carlo  
1108 methods (described in Sect. E in more  
1109 detail). Govaerts and Verstraete (1998)  
1110 demonstrated the use of a Monte Carlo ray  
1111 tracing (MCRT) model which considered the  
1112 internal structure of the leaf explicitly in 3D.  
1113 Baranoski (2006) developed a variant of  
1114 MCRT for bifacial leaves that calculates  
1115 Fresnel coefficients for all interfaces in the  
1116 leaf (air, adaxial and abaxial epidermis,  
1117 mesophyll cell walls and cytosol), and uses  
1118 these coefficients to weight Monte Carlo  
1119 samples of reflectance and transmittance;  
1120 scattering within a cell is approximated by  
1121 Beer's Law. The main advantage of these  
1122 more structurally detailed approaches is  
1123 flexibility. The main limitation is the

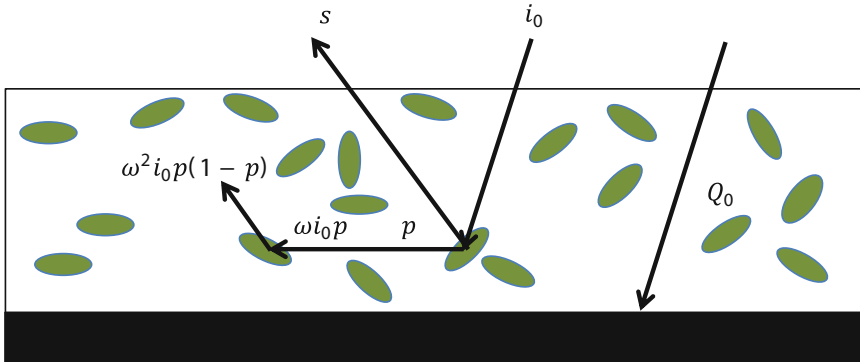


Fig. 11.5. Schematic representation of radiation that passes through the canopy uncollided ( $Q_0$ ), or is first intercepted by the canopy ( $i_0$ ) or escapes in the upward direction ( $s$ ) to be measured.  $p$  is the probability of a scattered photon being re-intercepted and  $\omega$  is the leaf single scattering albedo (After Lewis, P. <http://www2.geog.ucl.ac.uk/~plewis/CEGEG065/rtTheoryPt1v1.pdf>)

1124 requirement for information to parameterize  
 1125 the model, such as cell dimensions, air  
 1126 volumes etc. Such models can be used to  
 1127 explore the impact of structure at the canopy  
 1128 level on issues such as the relative absorption  
 1129 of diffuse to direct light (Alton et al. 2007;  
 1130 Brodersen et al. 2008), as well as at the leaf  
 1131 level, where surface and internal properties,  
 1132 such as polarization and focusing may be  
 1133 important (Martin et al. 1989; Combes  
 1134 et al. 2007).

1135 The following section describes relatively  
 1136 new developments in solving the canopy  
 1137 radiative transfer problem that have provided  
 1138 new parameterisations of multiple scattering  
 1139 that apply across scales from within-leaf  
 1140 to canopy. These methods have already  
 1141 been applied successfully to the problem of  
 1142 modelling leaf reflectance (Lewis and  
 1143 Disney 2007) and are providing new insight  
 1144 into the nature of radiative transfer in vege-  
 1145 tation more generally.

#### 1146 D. Recollision Probability and Spectral 1147 Invariance

1148 As seen above, the key to providing an accu-  
 1149 rate description of canopy radiative transfer  
 1150 is the multiple scattering component, particu-  
 1151 larly at NIR wavelengths. Development of  
 1152 the concept of the so-called 'recollision  
 1153 probability' ~~probability~~  $p$  has seen signifi-  
 1154 cant advancement in this area. The approach

is summarised in Huang et al. (2007), but is  
 based on the observation that the decrease in  
 scattered energy with increasing scattering  
 interactions is well-behaved and close to  
 linear in log space, at least in canopies with  
 low to moderate LAI (Lewis and Disney  
 1998). Scattered energy typically decreases  
 dramatically after 1 or 2 interactions, and  
 then proceeds to decrease more slowly with  
 increasing scattering order. This implies that,  
 once the scattering reaches the linearly  
 decreasing portion, the scattering at inter-  
 action order  $i + 1$  is simply  $p$  times the  
 scattering at interaction order  $i$ . Figure 11.5  
 illustrates this situation schematically.

From Fig. 11.5 we can see that some propo-  
 tion of the incoming radiation  $Q_0$  may  
 pass through uncollided to the lower bound-  
 ary layer. If this layer is assumed completely  
 absorbing (black soil, a reasonable approxi-  
 mation for dense understory and/or dark  
 soil), then multiple scattered radiation can  
 only originate from vegetation. The first  
 interaction with leaves is then  $i_0 = 1 - Q_0$ .  
 A fraction  $s$  of this scattered radiation exits  
 the canopy in the upward direction, and the  
 remaining proportion  $p$  interacts further with  
 leaves in the canopy. Therefore the first  
 order scattered radiation is  $s_1 = i_0 \omega (1-p)$   
 where  $\omega$  is the leaf single scattering albedo.  
 Rearranging, we obtain  $s_1/i_0 = \omega(1-p)$ . The  
 probability of being further intercepted is  
 also  $p$ , so the second order scattering

1188  $s_2 = \omega p s_1 = i_0 \omega^2 p(1-p)$ . Following the  
 1189 same logic for higher orders we see that

$$\begin{aligned} \frac{s}{i_0} &= \omega(1-p) + \omega^2(1-p)p + \omega^3(1-p)p^2 + \\ &\dots = \omega(1-p)[1 + \omega p + \omega^2 p^2 + \dots] \end{aligned} \quad (11.12)$$

1190 The series in  $p$  and  $\omega$  can be summed as

$$\frac{s}{i_0} = \frac{\omega(1-p)}{1-p\omega} \quad (11.13)$$

1191 This provides for a very compact description  
 1192 of multiple scattering, albeit under the  
 1193 assumptions of total scattering and black  
 1194 soil. Crucially, the resulting scattering is  
 1195 *independent of wavelength* i.e. is spectrally  
 1196 invariant, and is a function of  $p$  only, where  
 1197  $p$  is a purely structural term, encapsulating  
 1198 the size and arrangement of scattering  
 1199 elements within the canopy. Recollision the-  
 1200 ory has been developed over the last decade  
 1201 (Knyazikhin et al. 1998, 2011; Huang  
 1202 et al. 2007). It has been shown to work well  
 1203 for higher values of LAI when the understory  
 1204 becomes less important (Huang et al. 2007).  
 1205 This is also where optical EO tends to be less  
 1206 sensitive to variations in LAI. The recollision  
 1207 probability approach has now been used for a  
 1208 range of remote sensing applications includ-  
 1209 ing in a parameterised canopy model  
 1210 (Rautiainen and Stenberg 2005), to classify  
 1211 forest structural types (Schull et al. 2011),  
 1212 and for providing a structural framework for  
 1213 merging data from various sensors with dif-  
 1214 ferent spatial and spectral resolutions  
 1215 (Ganguly et al. 2008, 2012). Further, the  
 1216 same behaviour has been observed in atmo-  
 1217 spheric radiative transfer (Marshak  
 1218 et al. 2011).

1219 Specific insights provided from the spec-  
 1220 tral invariant approach include that of  
 1221 Smolander and Stenberg (2005) who showed  
 1222 that if the fundamental scattering element  
 1223 within a canopy is considered to be a shoot  
 1224 (a good approximations in conifers for  
 1225 example), then a shoot-level recollision  
 1226 probability  $p_{shoot}$ , can be defined. In this

1227 case total scattering can be expressed as a  
 1228 nested combination of the within-shoot  
 1229 needle-level recollision probability,  $p_{needle}$  and  
 1230  $p_{shoot}$ . This is a key insight into how different  
 1231 scales of clumping interact. Following this,  
 1232 Lewis and Disney (2007) used recollision  
 1233 probability to parameterise the PROSPECT  
 1234 leaf-level radiative transfer model. Their  
 1235 rephrasing in terms of  $p_{leaf}$  was able to repro-  
 1236 duce the behaviour of PROSPECT with very  
 1237 high accuracy (root mean square error  
 1238  $<0.4\%$  across all tested conditions). Lewis  
 1239 and Disney (2007) also showed that the same  
 1240 form of scattering will be nested across mul-  
 1241 tiple scales from within-leaf to shoot to can-  
 1242 opy. A key implication of this work was the  
 1243 observation that the structural and radiomet-  
 1244 ric components of the canopy (represented  
 1245 by  $p$  and the leaf absorbing constituents such  
 1246 as pigments, cellulose, lignin, and water) are  
 1247 fundamentally coupled. As a result Lewis  
 1248 and Disney (2007) conclude "... it is simply  
 1249 not possible to derive robust estimates of  
 1250 both leaf biochemical concentration and  
 1251 structural parameters such as LAI from  
 1252 (hyperspectral) data ... no matter how nar-  
 1253 row the wavebands or how many wavebands  
 1254 there are". Increasing LAI by some factor  
 1255  $k$  and simultaneously decreasing the bio-  
 1256 chemical concentration per unit leaf area by  
 1257 the same factor (i.e. keeping the total canopy  
 1258 concentration the same) can result in the  
 1259 same total scattering, but for a very different  
 1260 values of  $p$ , corresponding to very different  
 1261 canopy structures. This implies that without  
 1262 knowledge of either  $p$  or the leaf biochemi-  
 1263 cal constituents, independent retrieval of  
 1264 either from total scattering measurements is  
 1265 not possible. An additional implication is  
 1266 that attempts to estimate 'total' canopy bio-  
 1267 chemical concentration as a coupled mea-  
 1268 sure may contain large errors.

1269 The various developments of recollision  
 1270 probability have important implications for  
 1271 the use of Earth observation data to infer  
 1272 canopy biochemical properties, particularly  
 1273 pigment concentrations. Many studies have  
 1274 observed empirical correlations between  
 1275 canopy biochemical concentrations and  
 1276 observed spectral properties (reviewed by

1277 Ollinger 2011), including observed positive  
 1278 correlations between leaf nitrogen content  
 1279 per area (canopy N) and albedo. Such work  
 1280 suggests a potentially important route for  
 1281 monitoring canopy biochemistry (and hence  
 1282 state) from EO. However, recent work by  
 1283 Knyazikhin et al. (2013) building on  
 1284 recollision probability theory and the obser-  
 1285 vation that  $p$  encapsulates scattering across  
 1286 scales, shows quite clearly that some of these  
 1287 correlations e.g. between canopy N and  
 1288 albedo, are in fact entirely explained by can-  
 1289 opy structure. As an example, Knyazikhin  
 1290 et al. (2012) show that observed correlations  
 1291 between canopy N and reflectance can be  
 1292 almost completely explained by canopy  
 1293 structure. Knyazikhin et al. (2012) also sug-  
 1294 gest that canopy scattering can be  
 1295 reformulated using recollision probability,  
 1296 as a combination of separate structural and  
 1297 spectral terms as follows:

$$BRF_{\lambda}(\Omega) = DASF \cdot W_{\lambda} \quad (11.14)$$

1298 where  $DASF$  is the (structural) Directional  
 1299 Area Scattering Factor and  $W_{\lambda}$  is the (spec-  
 1300 tral) canopy scattering coefficient.  $DASF$  is  
 1301 defined as:

$$DASF = \rho(\Omega) \frac{i_0}{1 - p} \quad (11.15)$$

1302 where  $\rho(\Omega)$  is the directional gap density of  
 1303 the canopy, along a given viewing direction  
 1304  $\Omega$ ;  $i_0$  is the first interception by the canopy  
 1305 from Eq. 11.14.  $W_{\lambda}$  is defined as:

$$W_{\lambda} = \hat{\omega}_{\lambda} \frac{1 - p_{i_L}}{1 - \hat{\omega}_{\lambda} p_{i_L}} \quad (11.16)$$

1306 where  $i_L$  is the leaf interceptance defined as  
 1307 the fraction of radiation incident on the leaf  
 1308 that enters the leaf interior; and  $\hat{\omega}_{\lambda} = \omega_{\lambda}/i_L$ .  
 1309 The quantity  $\rho(\Omega)LAI$  is the fraction of leaf  
 1310 area inside the canopy visible from outside  
 1311 the canopy along  $\Omega$ . For dense canopies in  
 1312 the NIR,  $DASF(\Omega)LAI$  and is an estimate  
 1313 of the ratio between the leaf area that forms  
 1314 the canopy boundary as seen along  $\Omega$  and the

total (one-sided) leaf area, effectively the  
 'texture' of the canopy upper boundary.  
 Importantly, calculating  $DASF$  allows the  
 impact of structure to be removed from  
 observed hyperspectral reflectance, provid-  
 ing a potential route for re-analysis of empir-  
 ical relationships between biochemistry and  
 reflectance.

The recollision probability theory has  
 provided new ways to express scattering  
 across scales, and has found a range of  
 potential applications in accounting for  
 structural effects in EO measurements.  
 Ustin (2013) highlights the importance of  
 using a first principles radiative transfer  
 approach to accounting for the impact of  
 structure on EO estimates of biochemistry.

### E. 3D Monte Carlo Approaches

The methods outlined above to solve the  
 radiative transfer problem in vegetation  
 involve a range of approximations regarding  
 structural and radiometric properties in order  
 to make the problem tractable. A sub-class of  
 methods exist which solve the radiative  
 transfer problem based on 'brute force'  
 Monte Carlo sampling of the radiation field  
 in a 3D canopy. These methods derive from  
 developments in computer graphics, where  
 they form the basis of modern movie anima-  
 tion and special effects. The aim in these  
 applications is to simulate 'realistic' light  
 environments i.e. scenes that are either con-  
 vincing and/or aesthetically pleasing to the  
 human eye. For EO applications, the require-  
 ment is somewhat different i.e. physical  
 accuracy (including constraints such as  
 energy conservation for example). Monte  
 Carlo methods are computationally inten-  
 sive, which has tended to limit their applica-  
 tion. However, computing power has reached  
 a level where such limitations are no longer  
 so relevant, and these methods have some  
 key advantages for quantitative applications.  
 Niinemets and Anten (2009) discuss the  
 issues of the trade-off between accuracy  
 and efficiency in radiative transfer modelling  
 approaches.

1362 Monte Carlo methods in remote sensing  
1363 are reviewed in detail by Disney et al. (2000)  
1364 and Liang (2004). These methods fall into  
1365 two broad classes: radiosity (originating  
1366 from thermal engineering), which requires  
1367 calculating the viewed areas of each object  
1368 in a scene in relation to the other objects in  
1369 the scene (so-called 'view factors'); and ray  
1370 tracing (MCRT). I will briefly discuss the  
1371 latter method here, as it is more practical  
1372 for EO applications where view and illumi-  
1373 nation configurations change arbitrarily  
1374 (making radiosity less feasible). MCRT  
1375 essentially involves calculating the inter-  
1376 sections of photons (rays) projected into a  
1377 3D scene with the objects in the scene, and  
1378 determining the behaviour of these photons  
1379 at each intersection. The subsequent direc-  
1380 tion and energy of a scattered photon follow-  
1381 ing an intersection is governed by the  
1382 radiometric properties of absorption, trans-  
1383 mission and reflection of the surface at the  
1384 point of intersection, in addition to the geo-  
1385 metric scattering properties (phase function)  
1386 of the object. Objects are not limited to  
1387 representation by simple polygons (facets).  
1388 Volumetric objects can be used, in conjunc-  
1389 tion with a description of the (volumetric)  
1390 scattering properties of the materials  
1391 contained within (North 1996). Diffuse sam-  
1392 pling can be used to simulate diffuse light  
1393 sources (Govaerts 1996; Lewis 1999). The  
1394 bidirectional reflectance of a given scene  
1395 (represented as a collection of 3D objects)  
1396 is simulated by simply repeating the sam-  
1397 pling process for every sample (pixel) in  
1398 the viewing plane (Disney et al. 2000),  
1399 possibly multiple times.

1400 A key advantage of MCRT models is that  
1401 they can operate on structurally explicit 3D  
1402 scenes, often of arbitrary complexity,  
1403 allowing them to simulate EO signals with  
1404 the least possible number of assumptions  
1405 about structure. Some models represent  
1406 3D detail in a given scene down to the level  
1407 of individual needles and leaves (España  
1408 et al. 1999; Lewis 1999; Govaerts and  
1409 Verstraete 1998; Widlowski et al. 2006).  
1410 Other approaches represent larger structural  
1411 units explicitly such as tree crowns, but then

1412 make assumptions regarding the scattering  
1413 and extinction properties within individual  
1414 crowns (North 1996). The issue with this  
1415 latter approach is determining what these  
1416 within-crown bulk scattering properties  
1417 ought to be. Other models divide 3D space  
1418 into voxels, and assign voxel-average scatter-  
1419 ing properties, such as the Discrete Aniso-  
1420 tropic radiative transfer (DART) model of  
1421 Gastellu-Etchegorry et al. (2004). This has  
1422 benefits in terms of speed and simplicity, but  
1423 again at the expense of requiring definitions  
1424 of bulk (volume) scattering properties. Fully  
1425 explicit 3D MCRT models avoid these vol-  
1426 ume scattering approximations, but at the  
1427 expense of requiring 3D input on all canopy  
1428 elements, as well as potentially much greater  
1429 computational demands (Disney et al. 2006;  
1430 Widlowski et al. 2013).

1431 The ability to deal with 3D canopy struc-  
1432 ture explicitly means MCRT models are  
1433 ideally-suited to applications where we wish  
1434 to know, and have control over, 3D scene  
1435 properties in order to generate a modelled  
1436 EO signal e.g. for generating synthetic data  
1437 sets to test retrieval algorithms based on sim-  
1438 pler model approximations or when EO data  
1439 are not readily available. Disney et al. (2011)  
1440 show how 3D MCRT model simulations can  
1441 be used as a surrogate for observations of fire  
1442 impact. Other applications include simulating  
1443 the properties of new sensor characteristics  
1444 (Disney et al. 2009); understanding the  
1445 impact of structure on observations (España  
1446 et al. 1999); providing a common structural  
1447 framework for combining optical and micro-  
1448 wave scattering models (Disney et al. 2006);  
1449 and providing benchmark information for  
1450 testing simpler radiative transfer models  
1451 (Widlowski et al. 2007). This latter example  
1452 is an important one; a question that arises for  
1453 anyone using any radiative transfer approach  
1454 to an EO application is: which model is best  
1455 for my application, and why? The Radiation  
1456 Transfer Model Intercomparison exercise  
1457 (RAMI, [http://rami-benchmark.jrc.ec.europa.  
1458 eu/HTML/](http://rami-benchmark.jrc.ec.europa.eu/HTML/)) has sought to answer this ques-  
1459 tion via intercomparison of radiative transfer  
1460 models. Over various phases RAMI has  
1461 shown that detailed 3D MCRT models can

1462 provide the most credible solution to the  
 1463 radiative transfer problem in well-defined,  
 1464 simplified cases (Widlowski et al. 2007).  
 1465 Scenes can be defined for which MCRT  
 1466 models provide exact solutions (within  
 1467 limitations of numerical sampling), and  
 1468 this allows for testing of more approximate  
 1469 radiative transfer models, in particular  
 1470 quantifying the impact of model assump-  
 1471 tions on resulting model accuracy. The  
 1472 RAMI work has led to an online bench-  
 1473 marking tool, allowing radiative transfer  
 1474 model developers to test and benchmark  
 1475 their models (Widlowski et al. 2008). The  
 1476 most recent RAMI exercise has shown how  
 1477 detailed 3D MCRT models can represent the  
 1478 effects of structure on the EO signal for  
 1479 very complex (realistic) 3D scenes in ways  
 1480 that simpler models cannot (Widlowski  
 1481 et al. 2013).

1482 There are three main limitations of the  
 1483 MCRT approach. First, they are very slow  
 1484 compared to the more approximate models.  
 1485 This is certainly a problem if speed is abso-  
 1486 lutely essential, e.g. for large-scale or near  
 1487 real-time applications. MCRT models can of  
 1488 course still be used to quantify the impact  
 1489 of assumptions made in simpler models.  
 1490 Secondly, they cannot be inverted either  
 1491 directly or using standard optimisation  
 1492 routines, given their requirement for explicit  
 1493 location and properties of a (potentially)  
 1494 very large number of 3D objects. However,  
 1495 computation speeds have increased to an  
 1496 extent where it is now feasible to consider  
 1497 using a MCRT model for look-up table-  
 1498 based model inversion. It may take  
 1499 thousands of hours of CPU time to run for-  
 1500 ward MCRT model simulations over a large  
 1501 range of canopy, view and illumination  
 1502 configurations to populate the pertinent  
 1503 look-up tables, but these need only be run  
 1504 once. The third and perhaps most serious  
 1505 limitation of 3D MCRT models is that they  
 1506 are only as good as the underlying 3D scene  
 1507 descriptions on which they are based; the  
 1508 models require highly-detailed, accurate 3D  
 1509 structural information to generate 3D model  
 1510 scenes. This 3D information can come from  
 1511 various sources, including empirical growth

1512 models (e.g. España et al. 1999; Disney  
 1513 et al. 2006), purely parametric models  
 1514 (Widlowski et al. 2006; Disney et al. 2009),  
 1515 and parametric models modified using field  
 1516 measurements (Disney et al. 2011).

1517 A range of models can provide 3D scene  
 1518 information. Growth models provide an  
 1519 accurate description of a ‘domain-average’  
 1520 tree structure, but not a specific tree at a  
 1521 particular time (Leersnijder 1992; Perttunen  
 1522 et al. 1998). Parametric models allow a great  
 1523 degree of flexibility over manipulation of  
 1524 tree structure. Various models of this sort  
 1525 exist, e.g. xfrog (Xfrog Inc. xfrog.com) and  
 1526 OnyxTREE (Onyx Computing, onyxtree.  
 1527 com) and they have been used in EO  
 1528 applications (Disney et al. 2010, 2011).  
 1529 However, it can be both time-consuming  
 1530 and difficult to parameterise a model that is  
 1531 designed to ‘look right’ for computer graphic  
 1532 visualisation (Mêch and Prusinkiewicz  
 1533 1996), in such a way that it is a structurally  
 1534 accurate representation of a tree for radiative  
 1535 transfer applications (leaf and branch shape  
 1536 and size distributions, leaf angular  
 1537 distributions etc). An alternative approach  
 1538 is the use of growth grammars based on  
 1539 L-systems (Prusinkiewicz and Lindenmayer  
 1540 1990). These use simple growth rules to pro-  
 1541 duce ‘realistic’ canopy structure and have  
 1542 been used to drive 3D simulations, particu-  
 1543 larly of relatively simple crop canopies  
 1544 (Lewis 1999), but may bear little resem-  
 1545 blance to real canopies of greater complex-  
 1546 ity. Functional structural plant modelling  
 1547 (FSPM) overcomes this limitation to a cer-  
 1548 tain extent by considering fundamental rules  
 1549 of plant function due to the genetic and organ  
 1550 level constraints to drive structural develop-  
 1551 ment (Godin and Sinoquet 2005). The  
 1552 resulting 3D structure can in turn be  
 1553 expressed via L-systems. FSPM and  
 1554 L-systems approaches suffer from the same  
 1555 problem that the resulting models are accu-  
 1556 rate instances of a particular species or plant  
 1557 type, rather than specific (observed) plants.  
 1558 Furthermore, additional rules are needed to  
 1559 create a general, 3D scene.

1560 These limitations on 3D structure have led  
 1561 to [search](#) for new ways to derive detailed,



1562 accurate 3D information that can be used to  
1563 drive 3D simulation models. Some of these  
1564 methods are outlined below in Sect. IV.

### III. Effective Parameters

#### 1565 A. Basics: Definition of Effective 1566 Characteristics

1567 Having discussed the various approxi-  
1568 mations that can be employed to help solve  
1569 radiative transfer equations in leaves and  
1570 canopies, a note of caution is required in  
1571 regard to any biophysical parameters we  
1572 derive from EO data via such methods.

1573 For real canopies the exponent in Eq. 11.6  
1574 implicitly includes a structural term  $\zeta(\mu')$   
1575 encapsulating the fact that real canopies are  
1576 not turbid media but are clumped at multiple  
1577 scales from cm to tens of m). Leaves or  
1578 needles are arranged around twigs, along  
1579 branches, within crowns and within stands.  
1580 Pinty et al. (2004, 2006) suggest adopting an  
1581 effective LAI value  $LAI(\mu')$  i.e.

$$\widetilde{LAI}(\mu') = LAI\zeta(\mu') \quad (11.17)$$

1582 This permits a solution to the 1D limiting  
1583 case of radiative transfer in a 3D canopy that  
1584 is consistent with the assumptions made in  
1585 Eq. 11.2. Crucially however, the values of  
1586  $\widetilde{LAI}(\mu')$  are not the same as  $LAI$  which are  
1587 in turn, not the same as the actual LAI that  
1588 would be measured on the ground (unless  
1589 measured over some large, discrete canopy  
1590 volume). That is, the resulting radiative  
1591 transfer model parameters will be 'effective'  
1592 parameters and will not have a direct physi-  
1593 cally measurable meaning. These effective  
1594 parameters allow solution of the 1D radiative  
1595 transfer problem by representing domain-  
1596 averaged quantities that are forced to satisfy  
1597 the constraints associated with a 1D repre-  
1598 sentation of what is an inherently 3D system  
1599 (Pinty et al. 2006).

1600 The issue of effective parameters is  
1601 important because it encapsulates the prob-  
1602 lem of interpreting EO measurements more

generally. As an example, a typical use of a 1603  
1D radiative transfer scheme is to describe 1604  
the surface radiation budget in a large-scale 1605  
Earth System Model (ESM). Developing 1606  
such a model is inevitably a trade-off 1607  
between multiple and often competing 1608  
constraints including computational speed 1609  
and model robustness vs. providing 'suffi- 1610  
ciently accurate' radiant flux values (Pinty 1611  
et al. 2004). Moreover, introducing a 1612  
physically-realistic estimate of LAI (for 1613  
example) may only make things worse, as it 1614  
will not be consistent with the simplified 1615  
radiative transfer schemes and will thus 1616  
introduce errors. If radiative consistency is 1617  
the key requirement (getting the fluxes right) 1618  
rather than interpreting the LAI values, then 1619  
the effective parameters should be used 1620  
(Pinty et al. 2006, 2011a, b). What is true 1621  
of LAI is potentially true of other structural 1622  
and biochemical parameters in radiative 1623  
transfer schemes. 1624

The issue of consistency between 1625  
EO-derived biophysical parameters, and 1626  
their representation in models of vegetation 1627  
function, biogeochemical cycling and cli- 1628  
mate is key to making best use of both 1629  
observations and models. The fusion of EO 1630  
data with models, particularly via data 1631  
assimilation (DA), is a rapidly-growing 1632  
field because EO data can potentially provide 1633  
information on land cover, plant functional 1634  
types (PFTs), vegetation state and dynamics, 1635  
land surface temperature (LST), soil mois- 1636  
ture etc. at the scales and frequencies 1637  
required by the large-scale models (Pfeifer 1638  
et al. 2012). However, the further an 1639  
EO-derived parameter is away from a funda- 1640  
mental EO measurement, the more likely it is 1641  
to be 'effective' rather than directly measur- 1642  
able. This in turn increases the likelihood of 1643  
inconsistency between EO data and large- 1644  
scale models that use these parameters 1645  
(Carrer et al. 2012a; Pfeifer et al. 2012). 1646

#### B. Data Assimilation 1647

As the spatial detail of the land surface rep- 1648  
resentation within ESMs increases (from 1649  
 $\sim 10^3$  to  $\sim 10^1$  km and finer), the assumption 1650 [AU4](#)

1651 of canopy homogeneity typically assumed in  
 1652 a simplified radiative transfer approach is  
 1653 violated and potentially becomes an increas-  
 1654 ing source of error (Knorr and Heimann  
 1655 2001; Pinty et al. 2006; Brut et al. 2009;  
 1656 Widlowski et al. 2011). Various solutions  
 1657 have been proposed, essentially approaching  
 1658 the problem from opposite directions. From  
 1659 the EO perspective, one approach is to  
 1660 ensure consistency between EO parameters  
 1661 and ESMs as far as possible by coupling a  
 1662 physically-realistic radiative transfer scheme  
 1663 directly to the ESM that will use it. The ESM  
 1664 can then actually predict an EO measure-  
 1665 ment, which in turn allows direct comparison  
 1666 with EO data. Perhaps more importantly, the  
 1667 model can also be used to assimilate EO data  
 1668 to estimate ESM model state properties (in  
 1669 an inverse scheme). This approach lies at the  
 1670 heart of data assimilation schemes with land  
 1671 surface models (Quaife et al. 2008; Lewis et  
 1672 al. 2012). For a DA scheme, the RT models  
 1673 are referred to as ‘observation operators’  
 1674 (denoted  $H(\mathbf{x})$ ) which map the model state  
 1675 variable vector  $\mathbf{x}$  to the EO signal (as a vec-  
 1676 tor)  $\mathbf{R}$  for a given set of control variables i.e.  
 1677  $\mathbf{R} = H(\mathbf{x})$ . The inverse problem is then to  
 1678 obtain an estimate of some function of  $\mathbf{x}$ ,  $F$   
 1679 ( $\mathbf{x}$ ) from measurements  $\mathbf{R}$  (Lewis et al.  
 1680 2012). An advantage of this approach is  
 1681 that it can utilise much more direct EO  
 1682 measurements (reflectance or even  
 1683 radiance) where the uncertainties in the  
 1684 measurements can be better-characterised.  
 1685 This characterisation of uncertainty (in  
 1686 observation *and* radiative transfer model  
 1687 schemes) is critical for data assimilation.  
 1688 A drawback is that more complex radiative  
 1689 transfer schemes tend to slow the assimila-  
 1690 tion process, potentially limiting them for  
 1691 large-scale inverse problems (at least  
 1692 currently). However, data assimilation  
 1693 approaches of this sort are being used to  
 1694 assimilate EO data from a range of sources,  
 1695 and have shown great promise in improving  
 1696 and constraining model estimates of C fluxes  
 1697 and photosynthesis (Quaife et al. 2008;  
 1698 Knorr et al. 2010), evapotranspiration  
 1699 (Olioso et al. 2005), surface energy balance  
 1700 (Qin et al. 2007; Pinty et al. 2011a, b)

and hydrology (Rodell et al. 2004; Houser 1701  
 et al. 2012). 1702

### C. Scale Differences and Model 1703 Intercomparisons 1704

From the other direction, we can modify 1705  
 the ESM internal radiative transfer scheme 1706  
 to account for inconsistency with EO 1707  
 measurements and ensure the resulting 1708  
 ESM outputs are consistent at some broader, 1709  
 integrated level e.g. such as total productiv- 1710  
 ity (Brut et al. 2009; Carrer et al. 2012). An 1711  
 example of this is improved representation of 1712  
 canopy diffuse fluxes, which tend to increase 1713  
 C uptake (via increased photosynthesis) with 1714  
 increasing diffuse radiation fraction 1715  
 (Mercado et al. 2009). Carrer et al. (2012) 1716  
 show that introducing clumping to an ESM 1717  
 representation of vegetation (resulting in an 1718  
 effective LAI), even at coarse scale, can 1719  
 improve modelled annual GPP fluxes of var- 1720  
 ious deciduous and conifer forests by up to 1721  
 15–%. This approach accepts that the 1722  
 resulting internal model parameters are 1723  
 effective and not measurable in practice. 1724  
 Lafont et al. (2012) show that this modifica- 1725  
 tion of LAI can have a significant impact on 1726  
 the way fluxes are apportioned within differ- 1727  
 ent ESMs. 1728

An additional complication can arise that 1729  
 different internal LAI representations can 1730  
 cause processes such as photosynthesis and 1731  
 transpiration to reach different equilibria 1732  
 (different spatial and temporal distribution 1733  
 of fluxes) in different ESMs while still pro- 1734  
 ducing similar net C fluxes i.e. the models 1735  
 can arrive at the same answers for different 1736  
 reasons. This in turn can result in differences 1737  
 in seasonal variations (e.g. timing of peak 1738  
 fluxes) and/or longer-term model divergence 1739  
 that may be hard to identify (Richardson et 1740  
 al. 2012). The effective nature of the model 1741  
 parameters also makes model intercompari- 1742  
 son difficult. Clearly, the consideration of 1743  
 scale is not consistent between models. 1744

Recent work by Widlowski et al. (2011) 1745  
 has attempted to address the issue of 1746  
 consistency of radiative transfer schemes 1747  
 in ESMs systematically, by instigating a 1748

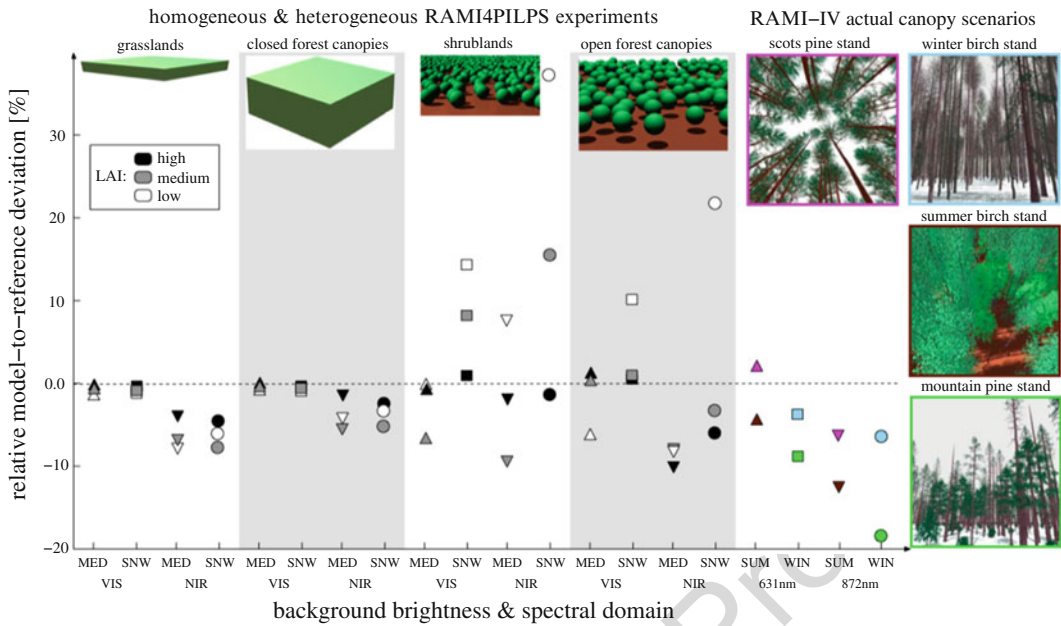


Fig. 11.6. An illustration of differences in canopy absorption as a function of increasing structural complexity (from left to right) for visible and NIR spectral domains. Different grey levels show varying LAI (low = 0.5, medium = 1.5, high = 2.5), over snow-covered (SNW) and medium-bright (MED) backgrounds, with  $\theta_i = 60^\circ$  or  $27^\circ$  respectively. The first two panels represent simple 1D radiative transfer models; the second two panels represent the most basic level of 3D heterogeneity; the right-most column includes four reference cases derived via a full 3D Monte Carlo Ray Tracing (MCRT) model description (Modified from Widlowski et al. (2011) © Wiley)

1749 radiative transfer model intercomparison  
 1750 exercise, RAMI4PILPS (<http://rami-bench>  
 1751 [mark.jrc.ec.europa.eu/HTML/RAMI4PILPS/](http://mark.jrc.ec.europa.eu/HTML/RAMI4PILPS/)  
 1752 [RAMI4PILPS.php](http://RAMI4PILPS.php)). RAMI4PILPS builds on  
 1753 both the RAMI exercise and the Project for  
 1754 Intercomparison of Land Surface Parameter-  
 1755 ization Schemes (PILPS). PILPS was set up  
 1756 to improve understanding of model pro-  
 1757 cesses in coupled climate, atmospheric and  
 1758 ESMS mainly through intercomparison of  
 1759 the various model parameterisation  
 1760 schemes (<http://www.pilps.mq.edu.au/>). PILPS  
 1761 recognises that for large, complex models, the  
 1762 wide range of approximations and possible  
 1763 parameterisations required makes direct  
 1764 model-to-model comparisons very difficult  
 1765 and instead compares the abilities of the models  
 1766 to reproduce various observed climate and land-  
 1767 surface trends (Henderson-Sellers et al. 2003).  
 1768 RAMI4PILPS is perhaps much closer to RAMI  
 1769 than PILPS in terms of the intercomparison  
 1770 approach. It attempts to isolate the radiative

1771 transfer schemes in participating models in  
 1772 such a way as to examine only that part,  
 1773 making like-for-like comparisons much more  
 1774 feasible over specific scenarios. In this case the  
 1775 RAMI results are used to provide a ‘known’  
 1776 reference solution. RAMI4PILPS covers quite  
 1777 a large range of model types, from simple land  
 1778 surface model schemes, to very complex  
 1779 models that describe the full range of surface  
 1780 energy, water and C fluxes between the surface  
 1781 and atmosphere. Figure 11.6 shows a comparison  
 1782 of the RAMI4PILPS models against the  
 1783 reference solution for a range of canopy  
 1784 complexities. This comparison demonstrates  
 1785 that the relatively simplistic concept of canopy  
 1786 ‘structure’ (from varying 1D homogeneous, to  
 1787 a simplified consideration of clumping) can  
 1788 still introduce a large degree of scatter between  
 1789 the models, as well as between the models and  
 1790 the reference solution under different environ-  
 1791 mental conditions and for different spectral  
 1792 regions.

**IV. New Observations of Structure and Function**

1794 Lastly, I discuss newer Earth observation  
 1795 techniques that provide rapid and detailed  
 1796 information on canopy structure and func-  
 1797 tion. These new technologies based on lidar  
 1798 (light detection and ranging) and micro-  
 1799 wave RADAR (radio detection and rang-  
 1800 ing) are becoming increasingly **more**  
 1801 widely available. I show that lidar is a  
 1802 near-direct remote sensing measurement  
 1803 of canopy height and structure. There is  
 1804 significant promise in merging airborne  
 1805 lidar scanning (ALS) instruments, and ter-  
 1806 restrial laser scanning (TLS) instruments,  
 1807 as well as optical and RADAR data in  
 1808 order to maximise structural information.  
 1809 The 3D nature of the lidar signal also raises  
 1810 the possibility of using these data to further  
 1811 extend and exploit the recollision probabil-  
 1812 ity approach to the canopy radiative trans-  
 1813 fer problem.

I also briefly consider the prospects  
 for EO data of this sort over the next  
 decade, and how such observations might  
 be used. Having discussed new structural  
 measurements, I turn lastly to a new mea-  
 surement related to canopy function based  
 on chlorophyll fluorescence.

*A. Structural Information from Lidar and RADAR*

Lidar systems have become increasingly  
 common over the last decade. Figure 11.7  
 illustrates this by highlighting the increase  
 in published papers with the words “lidar”  
 and “vegetation” in the title or abstract, from  
 1990–2012. The advent of airborne lidar  
 scanning (ALS) instruments, terrestrial  
 laser scanning (TLS) instruments, and the  
 lifespan of the only spaceborne lidar mission  
 to date used for terrestrial applications  
 (NASA ICESAT/Glas) are marked on the  
 figure (Fig. 11.7).

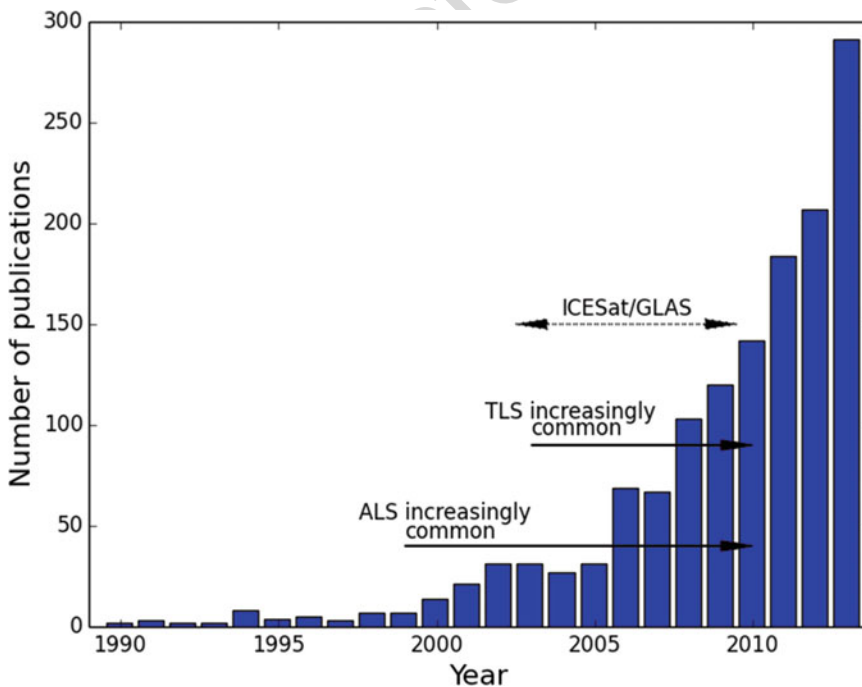


Fig. 11.7. Number of publications containing the words ‘lidar’ and ‘vegetation’ in the title or abstract from 1990 to 2013 (Citation information from Thomson Reuters Web of Knowledge ©). ALS and TLS are airborne and terrestrial lidar scanning respectively

1835 Lidar is an active remote sensing method,  
 1836 recording return time-of-flight of a laser  
 1837 pulse between instrument and target. Lidar  
 1838 provides a (near) direct estimate of surface  
 1839 (canopy) height and is in this sense a much  
 1840 more direct measurement than those relying  
 1841 on passive reflected or emitted radiation.  
 1842 Lidar instruments also record returned signal  
 1843 intensity and, in combination with height,  
 1844 this signal can provide unique information  
 1845 on the vertical distribution of canopy struc-  
 1846 ture when operated from above the canopy  
 1847 (e.g. Dubayah and Drake 2000). As  
 1848 discussed above, structure plays a critical  
 1849 role in radiative transfer in vegetation.  
 1850 Thus, structure must be accounted for to  
 1851 allow retrieval of canopy state and function  
 1852 from remote sensing. Lidar has proven  
 1853 extremely useful in addressing this issue  
 1854 (Lefsky et al. 2002; Armston et al. 2013a).

1855 *1. Discrete-Return Lidar Systems*

1856 Lidar systems broadly fall into one of  
 1857 two categories – discrete-return, or full-  
 1858 waveform (the less widely-used phase-  
 1859 based systems are not discussed here).  
 1860 Discrete return lidar essentially records the  
 1861 distance to the first object from which a  
 1862 return is recorded at the sensor, over some  
 1863 signal threshold, or multiple thresholds.  
 1864 Assuming that emitter and detector are  
 1865 co-located, the time-of-flight to the target is  
 1866  $t = 2d/c$  where  $d$  is the distance to the target,  
 1867 and  $c$  is the speed of light (and assuming that  
 1868 emitter and detector are co-located). For a  
 1869 sensor above a vegetation canopy returns  
 1870 may come from both the canopy and the  
 1871 ground, depending on canopy cover. It is  
 1872 then possible to determine the height of the  
 1873 vegetation canopy,  $h$ , through the difference  
 1874 in travel time between the two returns i.e.  
 1875  $h = (t_1 - t_2)c/2$ . Discrete return lidar datasets  
 1876 therefore comprise ‘point clouds’, each of  
 1877 which has a 3D co-ordinate relating its loca-  
 1878 tion to the sensor. Lidar has been widely  
 1879 used in this way to estimate biomass via  
 1880 allometric relationships with canopy height  
 1881 (e.g. Asner et al. 2010; Asner and Mascaro  
 1882 2014). Lidar measurements can be used to

estimate biomass over dense, high biomass 1883  
 (high LAI) tropical forests where passive 1884  
 optical measurements saturate and are 1885  
 thus insensitive to change and/or variation 1886  
 (Saatchi et al. 2011). Canopy height estima- 1887  
 tion from lidar is now included in routine 1888  
 commercial and forestry measurements 1889  
 (Næsset et al. 2004; Hyypä et al. 2008). 1890

2. *Full-Waveform Lidar Systems* 1891

Waveform (often referred to as ‘full-wave- 1892  
 form’) lidar systems record a ‘binned’ and 1893  
 digitised version of the real intensity return 1894  
 detected by the sensor, resulting from an 1895  
 outgoing pulse of known form (Mallet and 1896  
 Bretar 2009). Waveform instruments record 1897  
 the intensity of the response at a certain 1898  
 sampling rate (this sampling and detector 1899  
 non-linearity mean that the measurement 1900  
 never are true *full-waveform*), while 1901  
 performing minimal pulse-detection methods. 1902  
 Waveform lidar is becoming prevalent in air- 1903  
 borne systems, even if they are in practice 1904  
 often used as discrete return systems with 1905  
 much of the intermediate waveform informa- 1906  
 tion being ignored. However, the power of 1907  
 waveform lidar is that it has the capability to 1908  
 record detailed information on the vertical 1909  
 distribution of canopy structure, and hence 1910  
 has a range of applications in remote sensing 1911  
 of vegetation including height and biomass 1912  
 (Dubayah et al. 2010), LAI (Tang et al. 2012) 1913  
 and canopy gap fraction (Armston et al. 1914  
 2013a). The waveform signal can not only 1915  
 identify where there is a surface, but also 1916  
 what the properties of that surface are. This 1917  
 is particularly relevant for example in 1918  
 distinguishing woody from leaf material. 1919  
 Figure 11.8 shows an example of a modelled 1920  
 full-waveform lidar return over a conifer 1921  
 canopy, and highlights the potential informa- 1922  
 tion content of the signal. 1923

3. *Limitations and Future Developments* 1924  
*of Lidar Systems* 1925

A current limitation of lidar is the lack of 1926  
 wide area coverage due to reliance on air- 1927  
 borne platforms. However, ALS survey costs 1928

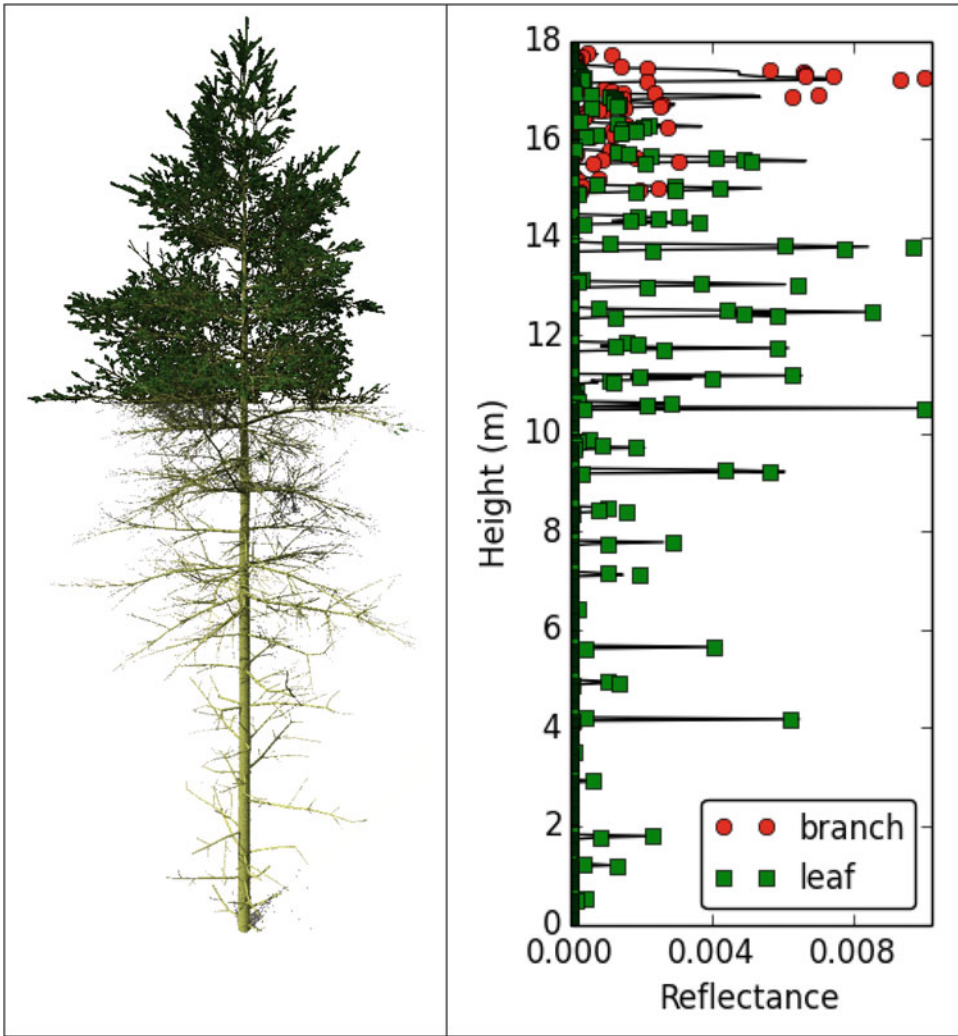


Fig. 11.8. Example of full-waveform lidar signal simulated from a 3D model of a Scots pine (*Pinus sylvestris*) tree (visualised in the left panel). The signal shows height-resolved return intensity (black impulses), as well as the normalized proportion of the signal in each height bin coming from the leaf and branch objects in the 3D model. Leaf and branch returns can be separated explicitly in the 3D model returns

1929 are coming down, and so larger and larger  
 1930 areas are being covered, with a number of  
 1931 countries now aiming to obtain total cover-  
 1932 age (e.g. see [http://www.gim-international.com/issues/articles/id1664-Swedish\\_Lidar\\_Project.html](http://www.gim-international.com/issues/articles/id1664-Swedish_Lidar_Project.html)). Obtaining this coverage is  
 1935 time-consuming (typically months to years)  
 1936 and hence can only provide a temporally  
 1937 fragmented ‘snapshot’ (note that this is only  
 1938 a limitation for very large areas; smaller  
 1939 regions, even 1000s of ha, where forest  
 1940 height and density will not vary in a few

1941 weeks or even months, can be covered rapidly and even revisited). In addition, these  
 1942 relatively large surveys are generally  
 1943 designed for deriving digital elevation  
 1944 models (DEMs) rather than for vegetation  
 1945 applications. As a result the sampling is  
 1946 often at or below  $1 \text{ pt m}^{-2}$  in order to reduce  
 1947 the survey time, meaning limited sampling  
 1948 of the canopy properties. A further difficulty  
 1949 is differentiating between leaf and woody  
 1950 material, particularly in larger footprint  
 1951 instruments. It has been proposed that this  
 1952

1953 limitation could be overcome by dual wave-  
 1954 length systems using spectral contrast to dis-  
 1955 tinguish canopy components (Morsdorf et al.  
 1956 2009). No system of this sort has been flown  
 1957 as yet, although work on laboratory  
 1958 prototypes show great promise (Woodhouse  
 1959 et al. 2011). An ongoing issue in dealing  
 1960 with lidar systems of all types is the often  
 1961 proprietary (and hence generally hidden)  
 1962 nature of the instrument characteristics  
 1963 (Disney et al. 2010). This makes it hard to  
 1964 obtain information on key technical  
 1965 specifications such as the thresholds used to  
 1966 trigger a recorded pulse (Armston et al.  
 1967 2013a), or the stability of the instrument  
 1968 absolute response (and gain). Lidar  
 1969 instruments are rarely if ever calibrated to  
 1970 provide absolute reflectance, making it hard  
 1971 to make quantitative comparisons of signal  
 1972 returns from different backgrounds and can-  
 1973 opy types.

1974 In terms of spaceborne lidar for vegeta-  
 1975 tion applications, unfortunately none cur-  
 1976 rently exist due to perceived cost and  
 1977 technical limitations. This is despite the suc-  
 1978 cess of NASA's ICESAT/Glas mission,  
 1979 which is remarkable given that it was not  
 1980 designed for vegetation applications and  
 1981 had some severe limitations including a  
 1982 large footprint (70 m), limited vertical reso-  
 1983 lution and relatively poor spatial sampling  
 1984 (hundreds of meters along tracks between  
 1985 footprints and kilometres between tracks  
 1986 horizontally). Despite this, Glas data have  
 1987 been widely used to derive estimates of can-  
 1988 opy height and structure over large areas,  
 1989 particularly for tall boreal and tropical  
 1990 forests (Harding and Carabajal 2005; Lefsky  
 1991 et al. 2005; Rosette et al. 2005) as well as  
 1992 forming the basis of the current best  
 1993 estimates of pan-tropical forest biomass  
 1994 (Saatchi et al. 2011; Baccini et al. 2012).  
 1995 A second ICESAT mission is due to launch  
 1996 in 2017 (<http://icesat.gsfc.nasa.gov/icesat2/>)  
 1997 but will have a different lidar system to  
 1998 that on ICESAT, and the possibilities for  
 1999 vegetation applications are as yet uncertain.  
 2000 Future prospects for space-based canopy  
 2001 lidar improved in July 2014, when NASA  
 2002 announced plans to launch the Global

Ecosystem Dynamics Investigation (GEDI) 2003  
 lidar system on board the International 2004  
 Space Station (ISS) in 2019. 2005

4. Terrestrial Laser Scanning (TLS) 2006

Another development over the last decade 2007  
 has been the rise of terrestrial laser scanning 2008  
 (TLS) instruments. Typically developed for 2009  
 commercial surveying applications, TLS 2010  
 data have proved an interesting source of 2011  
 3D canopy structure information (Maas et 2012  
 al. 2008). Given the importance of 3D struc- 2013  
 ture for radiative transfer modelling, bio- 2014  
 mass, canopy state etc., ways to rapidly and 2015  
 accurately characterise structure are obvi- 2016  
 ously attractive. This is particularly true as 2017  
 traditional field-based measurement of struc- 2018  
 ture are hard to make, particularly in remote 2019  
 and tall forests where access may be limited. 2020  
 Under these conditions, even measuring tree 2021  
 height can be problematic. As a result, struc- 2022  
 tural measurements are often limited to 2023  
 diameter-at-breast height, stem number den- 2024  
 sity, with perhaps some estimates of overall 2025  
 height, height-to-crown ratio, and crown 2026  
 extent. Tree height can be estimated 2027  
 using hypsometers or clinometers and even 2028  
 cheap laser ranging devices. However, for 2029  
 these height measurements, the top of a tree 2030  
 has to be visible from the ground. In dense 2031  
 canopies, with tall trees or in steep terrain, 2032  
 this can be problematic. Additional struc- 2033  
 tural measurements are often inferred 2034  
 from indirect techniques, such as gap frac- 2035  
 tion and cover (and hence LAI) from 2036  
 upward-looking hemispheric photographs. 2037  
 TLS can potentially overcome many of 2038  
 these limitations, allowing rapid estimation 2039  
 of dbh, height and vertical structure and 2040  
 potentially providing information that can 2041  
 be used to develop 3D canopy structural 2042  
 models quickly and accurately (Raumonen 2043  
 et al. 2013). 2044

The value of TLS measurements has seen 2045  
 development of new instruments specifically 2046  
 designed for vegetation applications, includ- 2047  
 ing: the use of wavelengths that are eye-safe, 2048  
 but also reflected strongly by vegetation (e.g. 2049  
 1064 nm); a move from discrete-return to 2050

2051 waveform instruments; full hemisphere  
2052 scanning; multiple wavelengths. Most of  
2053 these innovations have been developed in  
2054 the research community, but commercial  
2055 manufacturers are now recognising there  
2056 may be a larger market for robust field-portable  
2057 vegetation TLS instruments. Perhaps  
2058 the most exciting of these developments  
2059 is that of full-waveform, hemispherical  
2060 scanners, with dual wavelengths. The only  
2061 currently operational instrument is the  
2062 Salford Advanced Laser Canopy Analyser  
2063 (SALCA), which operates at 1040 and  
2064 1550 nm (Danson et al. 2014). As for ALS,  
2065 dual wavelengths have the potential to allow  
2066 leaf and woody material to be separated in  
2067 the lidar scans (Woodhouse et al. 2011).  
2068 Another new instrument is the dual-  
2069 wavelength Echidna laser scanner (DWEL,  
2070 Douglas et al. 2012), a development of the  
2071 Echidna single wavelength instrument that  
2072 has been deployed successfully for a number  
2073 of canopy applications (Yao et al. 2011).  
2074 Both SALCA and DWEL are prototypes  
2075 and require significant time to set up and  
2076 carry out full hemisphere scans. A more  
2077 robust, commercial alternative is the Riegl  
2078 VZ-400 scanner ([http://www.riegl.com/uploads/tx\\_pxpriegl/downloads/DataSheet\\_VZ-400\\_18-09-2013.pdf](http://www.riegl.com/uploads/tx_pxpriegl/downloads/DataSheet_VZ-400_18-09-2013.pdf)). This is a full  
2081 waveform hemispherical TLS instrument,  
2082 albeit with a single wavelength at 1550 nm.  
2083 It is a robust, field-ready instrument that can  
2084 carry out high angular resolution hemispherical  
2085 scans in 1–2 min. It can be used in  
2086 conjunction with a digital camera to provide  
2087 image data aligned to the scan data to aid  
2088 target identification (and even separation of  
2089 canopy elements). The instrument was not  
2090 designed for vegetation applications, and so  
2091 use of the waveform information for this  
2092 purpose is still in the early stages but is  
2093 potentially very promising (Disney et al.  
2094 2014). Field intercomparisons are being  
2095 used to test the various strengths and  
2096 weaknesses of the different instrument  
2097 approaches (Armston et al. 2013b).  
2098 A key obstacle of using TLS for 3D struc-  
2099 ture is transforming point cloud data  
2100 into some form of topologically-structured

description of individual trees, preferably in 2101  
a robust, automated way. Estimating tree 2102  
diameter at breast height and stem number- 2103  
density is fairly easy; height can be straight- 2104  
forward but requires points to be returned 2105  
from the top of the canopy, which can be 2106  
problematic in tall, dense canopies. Topol- 2107  
ogy is much harder, as it requires an associa- 2108  
tion between points and organs within a 2109  
particular tree (branches, leaves). Various 2110  
3D tree reconstruction methods have been 2111  
proposed for TLS data (e.g. Gorte and 2112  
Pfeifer 2004). Limitations of these methods 2113  
have been the speed and the requirement 2114  
for a large number of heuristic thresholds. 2115  
Recent work has shown that development of 2116  
more robust and rapid methods is possible 2117  
(Raumonen et al. 2013). 2118

2119 An additional problem for any reconstruc-  
2120 tion method is validation, given the practical  
2121 difficulty of measuring 3D structure for other  
2122 than the simplest trees. Detailed 3D radiative  
2123 transfer models as described above are proving  
2124 one possible route for overcoming this limita-  
2125 tion (Disney et al. 2012). In turn, the resulting  
2126 tree reconstructions open the way for routine  
2127 development of 3D scene models for remote  
2128 sensing simulations. Figure 11.9 shows an  
2129 example of a single TLS scan collected in an  
2130 Australian *Eucalyptus* forest. The rich struc-  
2131 tural nature of the data is immediately appar-  
2132 ent. Also shown are lidar ‘hits’ from a single  
2133 tree extracted from the resulting point cloud,  
2134 and a 3D reconstruction of the same tree via  
2135 the method of Raumonen et al. (2013). It is  
2136 worth noting that other uses of TLS are in  
2137 estimating canopy clumping and gap fraction  
2138 from the ground. TLS is potentially a more  
2139 accurate way to estimate clumping than e.g.  
2140 hemiphoto methods, as the effective resolution  
2141 is generally higher, and few if any assumptions  
2142 are required to estimate gap fraction (Casella  
2143 et al. 2013). Reconstruction of tree volume  
2144 from TLS data allows rapid, accurate and  
2145 non-destructive estimates of above ground bio-  
2146 mass to be made (Calders et al. 2014). The  
2147 TLS measurement errors are also independent  
2148 of tree size, unlike biomass estimates inferred  
2149 indirectly from tree height or diameter  
2150 measurements.



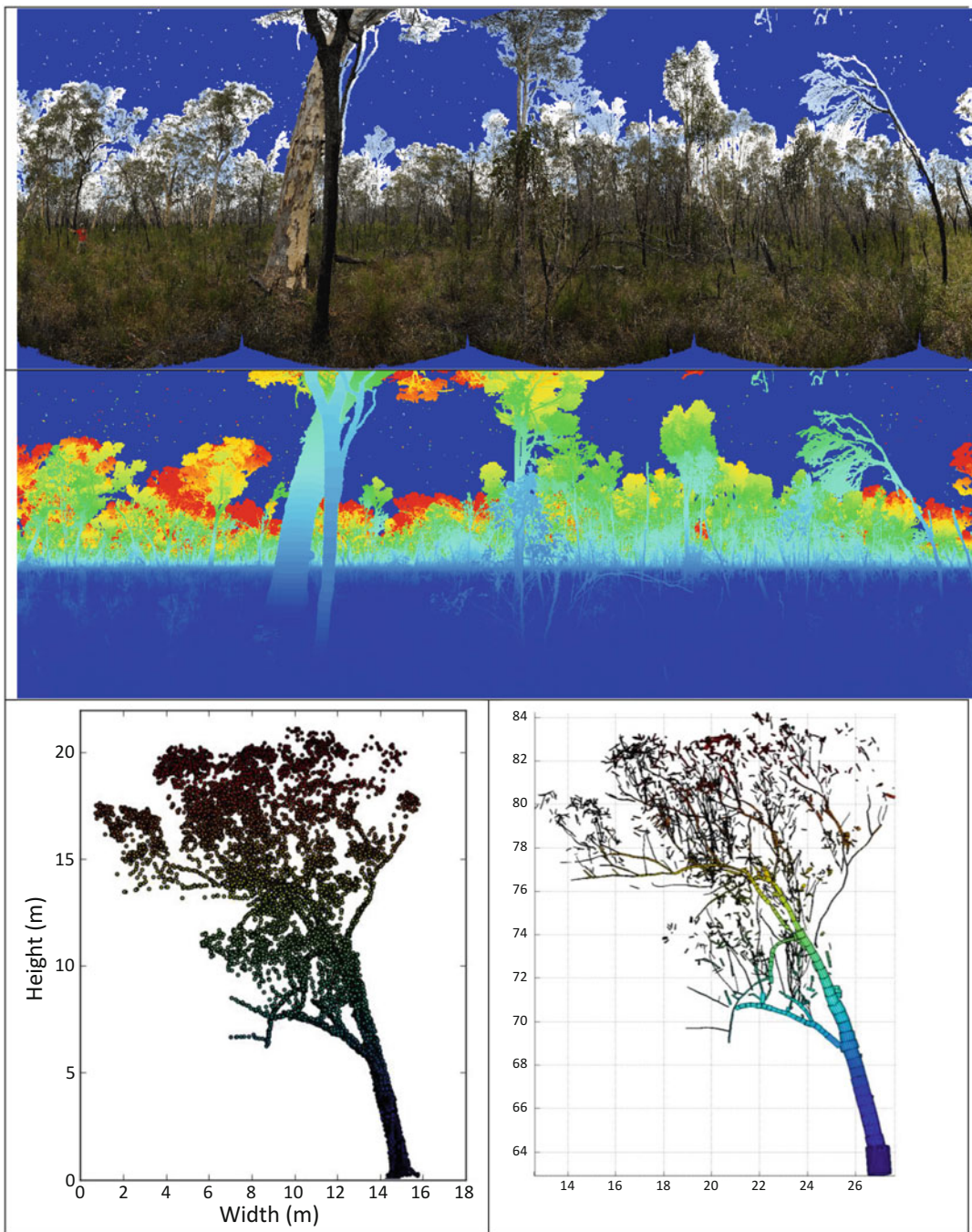


Fig. 11.9. Examples of Riegl VZ-400 terrestrial laser scanning (TLS) data from a bush site in Queensland, Australia and 3D tree structure reconstructed from the resulting scans. *Top*: 360° panorama of individual hemispheric photographs taken from a camera mounted on the TLS instrument. *Centre*: TLS scan, with height mapped to color. *Bottom left*: TLS points from a single tree extracted from the point cloud data (*color* represents height above the ground); *bottom right*: 3D reconstruction of the same tree (*color* again represents height) using the method of Raunonen et al. (2013)

## 2151 5. RADAR Systems

2152 RADAR is an alternative promising instru-  
 2153 ment for canopy structure and function  
 2154 observations (Lee and Pottier 2009). In fact,  
 2155 RADAR has its specific, very great,  
 2156 advantages over optical reflected methods  
 2157 of all-weather operation. Longer wavelength  
 2158 (tens of cm) RADAR is potentially sensitive  
 2159 to much higher levels of biomass due to  
 2160 penetration through the upper canopy and  
 2161 interacting only with larger trunks and  
 2162 branches. Unlike lidar systems, scanning  
 2163 imaging RADAR systems are well-advanced  
 2164 from an engineering perspective, allowing  
 2165 for the wide area coverage that is often  
 2166 such an advantage of remote sensing. High-  
 2167 resolution interferometric synthetic aperture  
 2168 RADAR (InSAR) instruments also hold  
 2169 promise for measurements of canopy height  
 2170 and structure (Krieger et al. 2007). However,  
 2171 the radiative transfer problem in the RADAR  
 2172 domain is less well-understood than for opti-  
 2173 cal wavelengths due to complications as a  
 2174 result of phase, polarization and coherence.  
 2175 As a result, exploitation of RADAR for  
 2176 vegetation applications has been primarily  
 2177 via empirical relationships between back-  
 2178 scatter and amount/biomass. Yet, these  
 2179 measurements are known to have significant  
 2180 shortcomings in terms of their ability to  
 2181 reliably predict biomass as a function of  
 2182 backscatter. This arises in part due to  
 2183 gaps in understanding of the physical  
 2184 processes governing the observed backscat-  
 2185 ter (Mitchard et al. 2011; Woodhouse  
 2186 et al. 2012).

## 2187 B. Fluorescence and Canopy Function

2188 Plant physiological stress studies mainly  
 2189 focus on pulse-modulated chlorophyll fluo-  
 2190 rescence, but the light levels needed for  
 2191 saturated pulses are far too high such that  
 2192 this method is not practical for EO  
 2193 (Schreiber et al. 1994; Baker 2008). As a  
 2194 potential alternative, there has been a major  
 2195 interest on solar-induced chlorophyll fluo-  
 2196 rescence ( $F_s$ ).  $F_s$  results from the excitation of  
 2197 chlorophyll molecules within assimilating

2198 leaves in the canopy and it is produced at  
 2199 the core of Photosystems I and II, primarily  
 2200 at photosystem II. Chlorophyll fluorescence  
 2201 is the remaining part of intercepted light  
 2202 energy, typically less than a few percent,  
 2203 that is not used photochemically nor  
 2204 dissipated non-photochemically. Fluores-  
 2205 cence occurs at longer wavelengths than the  
 2206 excitation light wavelength (typically  
 2207 650–800 nm for sunlight). Although  
 2208 minor,  $F_s$  is often inversely related to photo-  
 2209 synthesis, except when non-photochemical  
 2210 quenching of fluorescence occurs. Under  
 2211 stress, or in conditions where irradiance  
 2212 exceeds that required for photosynthesis,  
 2213 plant tissues increase heat production to dis-  
 2214 sipate excess energy. This tends to decrease  
 2215  $F_s$ , at least initially. Therefore, the resulting  
 2216 level of  $F_s$  is a balance between the radiation  
 2217 used for photosynthesis, heat production,  
 2218 and chlorophyll fluorescence. Steady-state  
 2219 measurements of  $F_s$  are therefore highly  
 2220 responsive to changes in environmental  
 2221 conditions and can be used as a  
 2222 near-direct indicator of plant photosynthetic  
 2223 function (Moya et al. 2004; Guanter et al.  
 2224 2012, 2014).

2225 This rapid response of  $F_s$  to changing  
 2226 environment (temperature, light) and canopy  
 2227 state (water, internal temperature, nutrients  
 2228 etc.) has elicited significant interest in the  
 2229 possibility of relating remotely sensed  
 2230 measurements of  $F_s$  to related canopy  
 2231 function and stress in particular. However,  
 2232 the induced fluorescence signal is only  
 2233 1–5 % of the total reflected solar signal in  
 2234 the NIR, making it difficult to separate from  
 2235 the background reflected signal (Meroni  
 2236 et al. 2009). Malenovsky et al. (2009) review  
 2237 some of the challenges to measuring  $F_s$  from  
 2238 the solar reflected signal. Despite these  
 2239 issues, there have been several attempts to  
 2240 employ these measurements, including the  
 2241 ESA FLEX (Fluorescence Explorer) mis-  
 2242 sion, primarily based on using narrow, spe-  
 2243 cific dark lines of the solar and atmospheric  
 2244 spectrum in which irradiance is strongly  
 2245 reduced (the so-called Fraunhofer lines).  
 2246 Three main Fraunhofer features have been  
 2247 exploited for  $F_s$  estimation: H $\alpha$  due to

2248 hydrogen (H) absorption (centred at  
2249 656.4 nm) and two telluric oxygen (O<sub>2</sub>)  
2250 absorption bands O2-B (687.0 nm) and  
2251 O2-A (760.4 nm). These lead to variants of  
2252 the so-called Fraunhofer Line Depth (FLD)  
2253 methods, in which  $F_s$  is estimated from some  
2254 form of ratio of the measured signal in a  
2255 Fraunhofer band to that measured in a refer-  
2256 ence band just outside the Fraunhofer band  
2257 (see Meroni et al. 2009 for details of these  
2258 methods). Key limitations for spaceborne  
2259 applications include the requirement for  
2260 very accurate spectral calibration, and the  
2261 removal of atmospheric and directional  
2262 effects. However, a major advantage of  
2263 exploiting existing (and future) imaging  
2264 spectroradiometers is that they have become  
2265 relatively common and acquire spatial image  
2266 data over wide areas. Guanter et al. (2007)  
2267 demonstrated that  $F_s$  retrieval was possible  
2268 from the MERIS sensor aboard ESA's  
2269 Envisat platform. Their approach incor-  
2270 porated  $F_s$  retrieval into an atmospheric radi-  
2271 ative transfer scheme so that  $F_s$  and surface  
2272 reflectance were retrieved consistently from  
2273 measured at-sensor radiance. This holds the  
2274 promise for more systematic retrievals from  
2275 newer sensors such as ESA's Sentinel 5 pre-  
2276 cursor mission, due for launch in 2015  
2277 ([http://esamultimedia.esa.int/docs/S5-prec\\_](http://esamultimedia.esa.int/docs/S5-prec_Data_Sheet.pdf)  
2278 [Data\\_Sheet.pdf](http://esamultimedia.esa.int/docs/S5-prec_Data_Sheet.pdf)).

2279 A new approach to retrieve  $F_s$  was  
2280 recently developed that does not rely on the  
2281 reflected solar signal, but uses estimates of  
2282 changes in the depth of solar Fraunhofer  
2283 lines, which tend to decrease due to  
2284 in-filling by  $F_s$  (Joiner et al. 2011;  
2285 Frankenberg et al. 2011a, b). These methods  
2286 rely on high spectral resolution observations  
2287 in the 755–775 nm range, which can resolve  
2288 individual Fraunhofer lines overlapping with  
2289 the  $F_s$  emission region. A key advantage of  
2290 this method is that Fraunhofer line depth is  
2291 unaffected by atmospheric scattering and  
2292 absorption in certain narrow spectral  
2293 windows. If these windows can be observed,  
2294 then it is possible to estimate the in-filling  
2295 due to  $F_s$  emission, which can of course only  
2296 arise from vegetation. Such an approach has

2297 only become feasible since the launch of the  
2298 Japanese Greenhouse Gases Observing  
2299 SATellite “IBUKI” (GOSAT), carrying the  
2300 Thermal and Near infrared Sensor for  
2301 carbon Observation (TANSO) ([http://www.gosat.nies.go.jp/index\\_e.html](http://www.gosat.nies.go.jp/index_e.html)). The TANSO  
2302 Fourier Transform Spectrometer (FTS) was  
2303 designed for measuring column-averaged  
2304 atmospheric CO<sub>2</sub> on global scales. The pos-  
2305 sibility for retrieving  $F_s$  was a serendipitous  
2306 after-thought. TANSO-FTS observations are  
2307 by no means ideal for  $F_s$  due to their large  
2308 spatial extent (tens km footprint), and lim-  
2309 ited spatial and temporal coverage due to the  
2310 instrument design. Despite these issues, the  
2311 first retrievals of  $F_s$  have shown large-scale  
2312 patterns consistent with expectations of sea-  
2313 sonal and regional variations in productivity  
2314 (Joiner et al. 2011). An example global map  
2315 of  $F_s$  derived from TANSO-FTS data is  
2316 shown in Fig. 11.10. 2317

2318 The results suggest that estimates of  $F_s$   
2319 correlate strongly with independent  
2320 estimates of GPP (Frankenberg et al.  
2321 2011b; Guanter et al. 2012, 2014). Critically,  
2322  $F_s$  also seems to contain information which  
2323 is independent of standard satellite  
2324 reflectance-derived estimates of productivity  
2325 via NDVI or EVI, for example, that basically  
2326 measure vegetation ‘greenness’ i.e. some  
2327 property related to vegetation amount. In  
2328 addition, the  $F_s$  signal is likely to be much  
2329 more sensitive to canopy stress due to its  
2330 origins in the photosynthetic machinery.  
2331 This might allow exploration of large-scale  
2332 impacts of stressors on vegetation productiv-  
2333 ity. As an example of this, Lee et al. (2013)  
2334 used satellite fluorescence to show that  
2335 instantaneous midday productivity (GPP)  
2336 was reduced by as much as 15 % across the  
2337 Amazon due to severe drought conditions in  
2338 2010. This interest in fluorescence as an  
2339 indicator of GPP has led to new ways to  
2340 exploit data from sensors primarily aimed  
2341 at atmospheric trace gas applications. Joiner  
2342 et al. (2013) have extracted fluorescence  
2343 from the Japanese GOME-2 instrument,  
2344 at higher precision and over smaller spatial  
2345 and temporal scales than is possible with

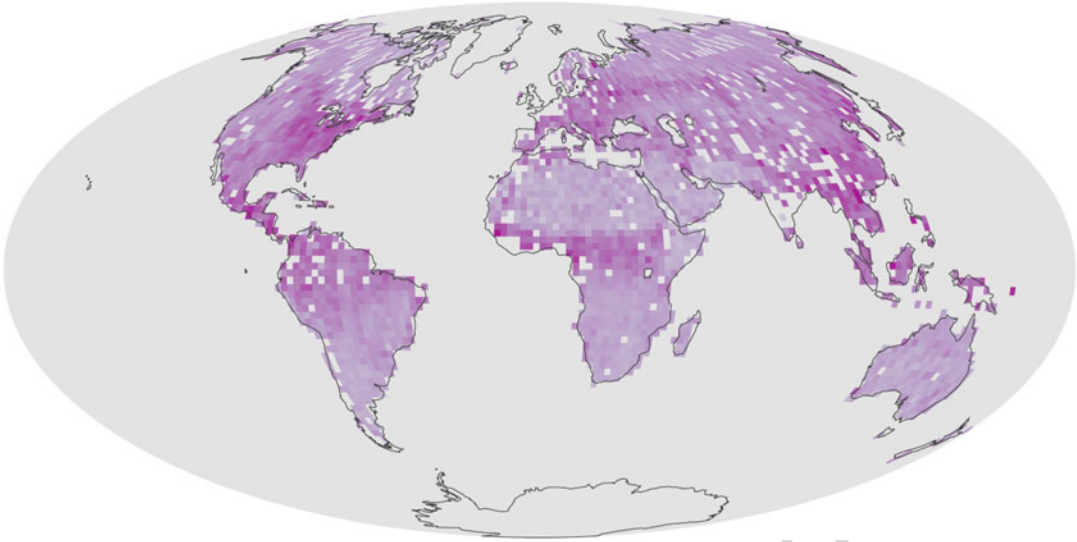


Fig. 11.10. Sun-induced steady-state fluorescence yield ( $F_s$ ) estimated from GOSAT TANSO-FTS observations composited during July 2009. Color intensity represents intensity of  $F_s$  in arbitrary units. Image from NASA Earth Observatory, created by Robert Simmon, using data from GOSAT (<http://visibleearth.nasa.gov/view.php?id=51121>)

2346 GOSAT. This work holds the promise of  
2347 more detailed maps of fluorescence from  
2348 space in the near future, which has in turn  
2349 led to an increase in interest as to how to  
2350 understand and exploit this signal using  
2351 models.

2352 The intriguing and unique information  
2353 content of  $F_s$  has led to work on modelling  
2354 the signal at the leaf and canopy levels in  
2355 order to understand the signal and potentially  
2356 allow parameter retrievals (Miller et al.  
2357 2005).  $F_s$  models rely on embedding a  
2358 model of leaf-level fluorescence within a  
2359 canopy reflectance model. The FLSAIL  
2360 model (Rosema et al. 1991) was an extension  
2361 of the SAIL canopy reflectance model  
2362 (Verhoef 1984) with  $F_s$  contributions  
2363 modelled through a doubling method. The  
2364 model was primarily developed for describ-  
2365 ing laser-induced rather than solar-induced  
2366 fluorescence. Olioso et al. (1992) used a  
2367 simple Beer's Law approximation for canopy  
2368 and leaf-level extinction and allowed for  
2369 within-canopy gradient in chlorophyll con-  
2370 tent to account for variations in leaf

biochemistry. The 3D DART model has  
also been modified to provide estimates of  
fluorescence at the canopy level (Miller et al.  
2005). FlurMODleaf is perhaps the most  
sophisticated  $F_s$  model, based on the PROS-  
PECT model described above (Miller et al.  
2005; Zarco-Tejada et al. 2006). This model  
has been used in various studies to show the  
influence of fluorescence on hyperspectral  
reflectance data (Zarco-Tejada et al. 2006,  
2009; Middleton et al. 2008).

Reliable remotely-sensed observations of  
fluorescence are still in their infancy but they  
hold out the tantalising prospect of much  
more direct estimates of canopy function,  
productivity, and stress than at present,  
from spaceborne instruments based on  
visible and near infra-red radiation reflectance.  
NASA's forthcoming Orbiting Carbon  
Observatory 2 (due to launch in mid-2014)  
may be capable of retrieving  $F_s$  from solar  
reflected signal, and there is increasing inter-  
est in other ways to retrieve  $F_s$  and vegeta-  
tion productivity from both spaceborne and  
airborne hyperspectral data.

## V. Conclusions

2396 Various issues arise in using remote sensing  
 2397 in estimating vegetation structure and func-  
 2398 tion in a quantitative sense. The primary  
 2399 limitation clearly is the indirect nature of  
 2400 most remote sensing measurements. How-  
 2401 ever, there are also great capabilities that  
 2402 now exist for mapping, even indirectly, can-  
 2403 opy state and function over wide areas and  
 2404 with repeated sampling allowing for studies  
 2405 of phenology, disturbance and anthropogenic  
 2406 impacts. We have explored the key role that  
 2407 vegetation structure plays in providing a  
 2408 link between incoming radiation and how  
 2409 this radiation is subsequently scattered or  
 2410 absorbed within the canopy before exiting  
 2411 to provide the remote sensing signal. New  
 2412 developments in understanding and model-  
 2413 ling the fundamental nature of these  
 2414 interactions are allowing us to chart a route  
 2415 from measurements made at the top-of-the  
 2416 atmosphere to estimates of canopy state and  
 2417 function. These developments are allowing  
 2418 us to unpick the relationships between  
 2419 'effective' canopy parameters, simplified or  
 2420 approximate manifestations of measurable  
 2421 physical parameters, and their real measur-  
 2422 able counterparts. Effective parameters  
 2423 allow us to model the radiation signal in  
 2424 practical, rapid models that are required to  
 2425 operate on global scales. The effective nature  
 2426 of the parameters, however, makes such  
 2427 models difficult to test and validate.  
 2428 Increases in the resolution and physical  
 2429 accuracy of large-scale land surface models  
 2430 has highlighted these discrepancies, but also  
 2431 calls for improvements in representations of  
 2432 vegetation. This is critical to reducing uncer-  
 2433 tainty in modelling the responses of terres-  
 2434 trial vegetation to changes in climate and  
 2435 land use, particularly via the terrestrial car-  
 2436 bon cycle.

2437 A range of new remote sensing  
 2438 measurements providing more direct infor-  
 2439 mation on canopy structure and function  
 2440 have been discussed. Terrestrial and airborne  
 2441 lidar systems, notably full-waveform and  
 2442 multispectral, are providing new information

on canopy structure. Observations of canopy  
 fluorescence have provided promising  
 estimates of canopy function, particularly  
 under stress. These new observations are  
 being exploited through developments in  
 detailed 3D canopy and leaf models, which  
 are making use of the continued increases in  
 computing power to reduce the requirements  
 for approximations.

From 2000 on there has been an unprece-  
 dented increase in high quality calibrated  
 consistent and error-quantified satellite  
 measurements of terrestrial vegetation at  
 resolutions of 250 m – 1 km, covering the  
 globe every few days. Notwithstanding  
 limitations, these observations are now central  
 to a huge range of applications. Indeed, many  
 of these observations have been identified as  
 so-called 'essential climate variables' ([http://  
 www.wmo.int/pages/prog/gcos/index.php?  
 name=EssentialClimateVariables](http://www.wmo.int/pages/prog/gcos/index.php?name=EssentialClimateVariables)).

However, the future is perhaps a little  
 more uncertain: current activities by major  
 space agencies include plans for continua-  
 tion of many, but not all, of the existing  
 observations of the land surface that have  
 proved so useful. Some of these new systems  
 will provide observations with reduced capa-  
 bility and/or scope than their predecessors,  
 for a variety of practical reasons. Given what  
 we have, and what is to come, we should  
 look forward to the coming decade as one  
 that will likely provide as many  
 developments in our ability to measure and  
 understand terrestrial vegetation as the last  
 decade undoubtedly had.

## Acknowledgments

I acknowledge the support of UCL Geogra-  
 phy and the NERC National Centre for Earth  
 Observation (NCEO), as well as the Univer-  
 sity of Queensland for hosting me during  
 some of this work. I also acknowledge vari-  
 ous colleagues for the numerous and varied  
 discussions over the last few years, that have  
 led to thoughts and collaborations on issues

2488 discussed here, including (inter alia): P  
 2489 Lewis, J Gomez-Dans, MJ Disney, M  
 2490 Barnsley, T Quaife, M DeKauwe, S  
 2491 Hancock, M Williams, S Quegan C Schaaf,  
 2492 A Strahler, Y Knyazkhin, B Pinty, JL  
 2493 Widlowski, J Armston and K Calders  
 2494 among many others. I am grateful to Prof.  
 2495 Vince Gutschick and the Mathematical  
 2496 Biosciences Institute of Ohio State Univer-  
 2497 sity, for the invitation to the MBI Workshop  
 2498 on Modelling Plant Development which  
 2499 provided initial impetus for this work.

## 2500 References

[AU5] 2501 Allen WA, Gausman HW, Richardson AJ, Thomas JR  
 2502 (1969) Interaction of isotropic light with a compact  
 2503 plant leaf. *J Opt Soc Am* 59:1376–1379  
 2504 Allen WA, Gausman HW, Richardson AJ (1970) Mean  
 2505 effective optical constants of cotton leaves. *J Opt*  
 2506 *Soc Am* 60:542–547  
 2507 Alton PB, North PRJ, Los SO (2007) The impact of  
 2508 diffuse sunlight on canopy light-use efficiency, gross  
 2509 photosynthetic product and net ecosystem exchange  
 2510 in three forest biomes. *Glob Chang Biol* 13:776–787  
 2511 Angert A, Biraud S, Henning CC, Bauermann W,  
 2512 Pinzon J, Tucker CJ, Fung I (2005) Drier summers  
 2513 cancel out the CO<sub>2</sub> uptake enhancement induced by  
 2514 warmer springs. *Proc Natl Acad Sci U S A*  
 2515 102:10823–10827  
 2516 Armston J, Disney MI, Lewis P, Scarth P, Phinn S,  
 2517 Lucas R, Bunting P, Goodwin N (2013a) Direct  
 2518 retrieval of canopy gap probability using airborne  
 2519 waveform lidar. *Remote Sens Environ* 134:24–38  
 2520 Armston J, Newnham G, Strahler AH, Schaaf C,  
 2521 Danson M, Gaulton R, Zhang Z, . . . , Wu S (2013b)  
 2522 Intercomparison of terrestrial laser scanning  
 2523 instruments for assessing forested ecosystems: a  
 2524 Brisbane field experiment, B11G-0443, In: *Proc.*  
 2525 *AGU San Francisco*, Dec. 2013 [http://128.197.168.](http://128.197.168.195/wp-content/uploads/2013/11/Armston_Brisbane.pdf)  
 2526 [195/wp-content/uploads/2013/11/Armston\\_Brisbane.](http://128.197.168.195/wp-content/uploads/2013/11/Armston_Brisbane.pdf)  
 2527 [pdf](http://128.197.168.195/wp-content/uploads/2013/11/Armston_Brisbane.pdf)  
 2528 Asner GP, Mascaro J (2014) Mapping tropical forest  
 2529 carbon: Calibrating plot estimates to a simple  
 2530 LiDAR metric. *Remote Sens Environ* 140:614–624  
 2531 Asner GP, Powell GV, Mascaro J, Knapp DE, Clark JK,  
 2532 Jacobson J, Kennedy-Bowdoin T, . . . , Hughes RF  
 2533 (2010) High resolution forest carbon stocks and  
 2534 emissions in the Amazon. *Proc Natl Acad Sci USA*  
 2535 107:16738–16742

Asrar G (ed) (1989) *Theory and Applications of Opti-* 2536  
*cal Remote Sensing.* Wiley, New York 2537  
 Baccini A, Goetz SJ, Walker WS, Laporte NT, Sun M, 2538  
 Sulla-Menashe D, Hackler J, . . . , Houghton RA 2539  
 (2012) Estimated carbon dioxide emissions from 2540  
 tropical deforestation improved by carbon-density 2541  
 maps. *Nat Clim Change* 2:182–185 2542  
 Baranoski GVG (2006) Modeling the interaction of 2543  
 infrared radiation (750 to 2500 nm) with bifacial 2544  
 and unifacial plant leaves. *Remote Sens Environ* 2545  
 100:335–347 2546  
 Best MJ, Pryor M, Clark DB, Rooney GG, Essery 2547  
 RLH, Ménard CB, Edwards JM, . . . , Harding RJ 2548  
 (2011) The Joint UK Land Environment Simulator 2549  
 (JULES), model description – Part 1: Energy and 2550  
 water fluxes. *Geosci Model Dev* 4:677–699 2551  
 Brando P, Goetz S, Baccini A, Nepstad DC, Beck PSA, 2552  
 Christman MC (2010) Seasonal and interannual 2553  
 variability of climate and vegetation indices across 2554  
 the Amazon. *Proc Natl Acad Sci U S A* 2555  
 107:14685–14690 2556  
 Brodersen CR, Voglemann TC, Williams WE, Gorton 2557  
 H (2008) A new paradigm in leaf-level photosynthe- 2558  
 sis: direct and diffuse lights are not equal. *Plant Cell* 2559  
*Environ* 31:159–164 2560  
 Bunnik NJJ (1978) The multispectral reflectance 2561  
 of shortwave radiation of agricultural crops in rela- 2562  
 tion with their morphological and optical properties. 2563  
 PhD Thesis, In *Mededelingen Landbouwhoge-* 2564  
*school, Wageningen University, Wageningen* 2565  
 Brut A, Rüdiger C, Lafont S, Roujean J-L, Calvet J-C, [AU6] 2566  
 Jarlan L, Gibelin A-L, . . . , Ceschi E (2009) 2567  
 Modelling LAI at a regional scale with ISBA-A- 2568  
 gs: comparison with satellite-derived LAI over 2569  
 southwestern France. *Biogeosciences* 6:1389–1404 2570  
 Calders K, Newnham G, Burt A, Murphy S, 2571  
 Raunonen P, Herold M, Culvenor D, . . . , Kaasalainen 2572  
 M (2014) Non-destructive estimates of above-ground 2573  
 biomass using terrestrial laser scanning. *Methods* 2574  
*Ecol Evol*, in press. doi: [10.1111/2041-210X.12301](https://doi.org/10.1111/2041-210X.12301) 2575  
 Campbell GS (1986) Extinction coefficient for radia- 2576  
 tion in plant canopies calculated using an ellipsoidal 2577  
 inclination angle distribution. *Agric For Meteorol* 2578  
 36:317–321 2579  
 Carrer D, Roujean JL, Lafont S, Boone A, Calvet, JC 2580  
 (2012) A vegetation radiative transfer scheme in 2581  
 ISBA-A-gs interactive vegetation model. In: 2582  
*Proceedings of IGARSS2012. Munich, Germany,* 2583  
 22–27 July 2012, pp 1151–1154 2584  
 Casella E, Disney MI, McKay H (2013) tLiDAR 2585  
 methodologies can overcome limitations in 2586  
 estimating forest canopy LAI from conventional 2587  
 hemispherical photograph analyses. In: *Proceedings* 2588

- 2589 of Functional Structural Plant Modelling 2013  
2590 (FSPM2013), Saariselkä, Finland, 9–14 June, 2013
- 2591 Cescatti A, Niinemets Ü (2004) Leaf to landscape. In:  
2592 Smith WK, Vogelmann TC, Critchley C (eds) Eco-  
2593 logical Studies: Photosynthetic Adaptation, vol 178.  
2594 Springer, New York, pp 42–85
- 2595 Chandrasekhar S (1960) Radiative Transfer. Dover,  
2596 New York
- 2597 Chapin FS III, Chapin MC, Matson PA, Vitousek P  
2598 (2011) Principles of Terrestrial Ecosystem Ecology,  
2599 2nd edn. Springer, New York
- 2600 Combes D, Bousquet L, Jacquemoud S, Sinoquet H,  
2601 Varlet-Grancher C, Moya I (2007) A new spectrogo-  
2602 niophotometer to measure leaf spectral and direc-  
2603 tional optical properties. *Remote Sens Environ*  
2604 109:107–117
- 2605 Danson FM, Gaulton R, Armitage RP, Disney MI,  
2606 Gunawan O, Lewis PE, Pearson G, Ramirez AF  
2607 (2014) Developing a dual-wavelength full-wave-  
2608 form terrestrial laser scanner to characterise forest  
2609 canopy structure. *Agric For Meteorol* 198–199:7–14
- 2610 Dawson TP, Curran PJ, Plummer SE (1998)  
2611 LIBERTY – modeling the effects of leaf biochemi-  
2612 cal concentration on reflectance spectra. *Remote*  
2613 *Sens Environ* 65:50–60
- 2614 Denman KL, Brasseur G, Chidthaisong A, Ciais P, Cox  
2615 PM, Dickinson RE, Hauglustaine D, . . . , Zhang X  
2616 (2007) Couplings between changes in the climate  
2617 system and biogeochemistry. In: Solomon S, Qin D,  
2618 Manning M, Chen Z, Marquis M, Averyt KB,  
2619 Tignor M, Miller HL (eds) *Climate Change 2007:*  
2620 *The Physical Science Basis. Contribution of*  
2621 *Working Group I to the Fourth Assessment Report*  
2622 *of the Intergovernmental Panel on Climate*  
2623 *Change.* Cambridge University Press, Cambridge,  
2624 pp 499–587
- 2625 Dickinson RE (1983) Land surface processes and cli-  
2626 mate—surface albedos and energy balance. *Adv*  
2627 *Geophys* 25:305–353
- 2628 Disney MI, Lewis P, North P (2000) Monte Carlo ray  
2629 tracing in optical canopy reflectance modelling.  
2630 *Remote Sens Rev* 18:163–197
- 2631 Disney MI, Lewis P, Quaife T, Nichol, C (2005) A  
2632 spectral invariant approach to modeling canopy  
2633 and leaf scattering. In: *Proceedings of the 9th Inter-*  
2634 *national Symposium on Physical Measurements and*  
2635 *Signatures in Remote Sensing (ISPMSRS), 17–*  
2636 *19 October 2005, Beijing, China, Part 1: 318–320*
- 2637 Disney MI, Lewis P, Saich P (2006) 3D modelling  
2638 of forest canopy structure for remote sensing  
2639 simulations in the optical and microwave domains.  
2640 *Remote Sens Environ* 100:114–132
- 2641 Disney MI, Lewis P, Bouvet M, Prieto-Blanco A,  
2642 Hancock S (2009) Quantifying surface reflectivity  
for spaceborne lidar via two independent methods. *IEEE Trans Geosci Remote Sens* 47:3262–3271
- Disney MI, Kalogirou V, Lewis PE, Prieto-Blanco A,  
Hancock S, Pfeifer M (2010) Simulating the impact  
of discrete-return lidar system and survey  
characteristics over 2 young conifer and broadleaf  
forests. *Remote Sens Environ* 114:1546–1560
- Disney MI, Lewis P, Gomez-Dans J, Roy D,  
Wooster M, Lajas D (2011) 3D radiative transfer  
modelling of fire impacts on a two-layer savanna  
system. *Remote Sens Environ* 115:1866–1881
- Disney MI, Lewis P, Raunonen P (2012) Testing a new  
vegetation structure retrieval algorithm from terres-  
trial lidar scanner data using 3D models. In:  
*Proceedings of Silvilaser 2012, Vancouver, BC,*  
Canada, 16–19 September 2012
- Douglas ES, Strahler AH, Martel J, Cook T, Mendillo  
C, Marshall R, Chakrabarti S, . . . , Lovell J (2012)  
DWEL: a dual-wavelength Echidna lidar for  
ground-based forest scanning. In: *Proceedings of*  
IGARSS2012, 22–27 July 2012, Munich, Germany,  
pp 4998–5001
- Dubayah RO, Drake JB (2000) Lidar remote sensing  
for forestry. *J For* 98:44–46
- España M, Baret F, Aries F, Andrieu B, Chelle M  
(1999) Radiative transfer sensitivity to the accuracy  
of canopy structure description. The case of a maize  
canopy. *Agronomie* 19:241–254
- Feret JB, François C, Asner GP, Gitelson AA,  
Martin RE, Bidet LPR, Ustin SL, le Maire G,  
Jacquemoud S (2008) PROSPECT-4 and 5:  
advances in the leaf optical properties model  
separating photosynthetic pigments. *Remote Sens*  
*Environ* 112:3030–3043
- Flerchinger GN, Yu Q (2007) Simplified expressions  
for radiation scattering in canopies with ellipsoidal  
leaf angle distributions. *Agric For Meteorol*  
144:230–235
- Frankenberg C, Butz A, Toon GC (2011a)  
Disentangling chlorophyll fluorescence from atmo-  
spheric scattering effects in O2A-band spectra of  
reflected sun-light. *Geophys Res Lett* 38, L03801
- Frankenberg C, Fisher JB, Worden J, Badgley G,  
Saatchi SS, Lee J-E, Toon GC, . . . , Yokota T  
(2011b) New global observations of the terrestrial  
carbon cycle from GOSAT: Patterns of plant fluo-  
rescence with gross primary productivity. *Geophys*  
*Res Lett* 38:L17706
- Fung AK (1994) *Microwave Scattering and Emission*  
*Models and Their Applications.* Artech House,  
Norwood
- Ganguly S, Schull MA, Samanta A, Shabanov NV,  
Milesi C, Nemani R, Knyazikhin YV, Myneni RB  
(2008) Generating vegetation leaf area index earth

- 2697 system data records from multiple sensors. Part 1:  
2698 Theory. *Remote Sens Environ* 112:4333–4343
- 2699 Ganguly S, Nemani R, Zhong G, Hashimoto H,  
2700 Milesi C, Michaelis M, Wang W, . . . , Myneni RB  
2701 (2012) Generating global leaf area index from  
2702 Landsat: algorithm formulation and demonstration.  
2703 *Remote Sens Environ* 122:185–202
- 2704 Gastellu-Etchegorry JP, Martin E, Gascon F (2004)  
2705 Dart: a 3D model for simulating satellite images  
2706 and studying surface radiation budget. *Int J Remote*  
2707 *Sens* 25:73–96
- 2708 Godin C, Sinoquet H (2005) Functional–structural  
2709 plant modelling. *New Phytol* 166:705–708
- 2710 Goel NS (1988) Models of vegetation canopy reflec-  
2711 tance and their use in the estimation of biophysical  
2712 parameters from reflectance data. *Remote Sens Rev*  
2713 4:1–222
- 2714 Goel NS, Strelbel DE (1984) Simple beta distribution  
2715 representation of leaf orientation in vegetation  
2716 canopies. *Agron J* 75:800–802
- 2717 Goel NS, Thompson RL (2000) A snapshot of canopy  
2718 reflectance models, and a universal model for the  
2719 radiation regime. *Remote Sens Rev* 18:197–225
- 2720 Gorte B, Pfeifer N (2004) Structuring laser-scanned  
2721 trees using 3D mathematical morphology. *Int Arch*  
2722 *Photogramm Remote Sens XXXV*:929–933
- 2723 Govaerts Y, Verstraete MM (1998) Raytran: a Monte  
2724 Carlo ray-tracing model to compute light scattering  
2725 in three-dimensional heterogeneous media. *IEEE*  
2726 *Trans Geosci Remote Sens* 36:493–505
- 2727 Grace J, Nichol C, Disney MI, Lewis P, Quaife T,  
2728 Bowyer P (2007) Can we measure photosynthesis  
2729 from space? *Glob Chang Biol* 13:1484–1497
- 2730 Guanter L, Alonso L, Gomez-Chova L, Amoros-  
2731 Lopez J, Moreno J (2007) Estimation of solar-  
2732 induced vegetation fluorescence from space  
2733 measurements. *Geophys Res Lett* 34:L08401
- 2734 Guanter L, Frankenberg C, Dudhia A, Lewis PE,  
2735 Gomez-Dans J, Kuze A, Suto H, Grainger RG  
2736 (2012) Retrieval and global assessment of terrestrial  
2737 chlorophyll fluorescence from GOSAT space  
2738 measurements. *Remote Sens Environ* 121:236–257
- 2739 Guanter L, Zhang Y, Jung M, Joiner J, Voigt M, Berry  
2740 JA, Frankenberg C, . . . , Griffis TJ (2014) Global and  
2741 time-resolved monitoring of crop photosynthesis  
2742 with chlorophyll fluorescence. *Proc Natl Acad Sci*  
2743 *USA* 111:E1327–E1333
- 2744 Harding DJ, Carabajal CC (2005) ICESat waveform  
2745 measurements of within-footprint topographic relief  
2746 and vegetation vertical structure. *Geophys Res Lett*  
2747 32, L21S10
- 2748 Henderson-Sellers A, Irannejad P, McGuffie K, Pitman  
2749 A (2003) Predicting land-surface climates: better  
2750 skill or moving targets? *Geophys Res Lett* 30:1777
- Hosgood B, Jacquemoud S, Andreoli G, Verdebout J,  
Pedrini G, Schmuck G (1995) LOPEX: Leaf optical  
properties experiment 93. Technical Report EUR  
16095 EN, Joint Research Center, European Com-  
mission, Institute for Remote Sensing Applications
- Houser P, De Lannoy G, Walker JP (2012) Hydrologic  
data assimilation. In: Tiefenbacher JP (ed)  
Approaches to Managing Disaster – Assessing  
Hazards, Emergencies and Disaster Impacts.  
InTech, Rijeka, 162 p
- Huang D, Knyazikhin Y, Dickinson R, Rautiainen M,  
Stenberg P, Disney MI, Lewis P, . . . , Myneni RB  
(2007) Canopy spectral invariants for remote sens-  
ing and model applications. *Remote Sens Environ*  
106:106–122
- Hyypä J, Hyypä H, Leckie D, Gougeonm F, Yu X,  
Maltamo M (2008) Review of methods of  
small-footprint airborne laser scanning for  
extracting forest inventory data in boreal forests.  
*Int J Remote Sens* 29:1339–1366
- Jacquemoud S, Ustin S (2008) Modelling leaf optical  
properties. *Photobiological Sciences Online* (Smith  
KC, ed.) American Society for Photobiology, [http://](http://www.photobiology.info/)  
[www.photobiology.info/](http://www.photobiology.info/)
- Jacquemoud S, Ustin SL, Verdebout J, Schmuck G,  
Andreoli G, Hosgood B (1996) Estimating leaf bio-  
chemistry using the PROSPECT leaf optical  
properties model. *Remote Sens Environ* 56:194–202
- Jacquemoud S, Verhoef W, Baret F, Bacour C, Zarco-  
Tejada PJ, Asner GP, Francois C, Ustin SL (2009)  
PROSPECT + SAIL Models: a review of use for  
vegetation characterization. *Remote Sens Environ*  
113:56–66
- Joiner J, Yoshida Y, Vasilkov AP, Yoshida Y, Corp LA,  
Middleton EM (2011) First observations of global  
and seasonal terrestrial chlorophyll fluorescence  
from space. *Biogeosciences* 8:637–651
- Joiner J, Guanter L, Lindstrot R, Voigt M, Vasilkov AP,  
Middleton EM, Huemmerich KF, . . . , Franenberg C  
(2013) Global monitoring of terrestrial chlorophyll  
fluorescence from moderate spectral resolution  
near-infrared satellite measurements: methodology,  
simulations and application to GOME-2. *Atmos*  
*Meas Tech Discuss* 6:3883–3930
- Jones HG (2014) *Plants and Microclimate: A Quanti-  
tative Approach to Environmental Plant Physiology*,  
3rd edn. CUP, Cambridge
- Jones HG, Vaughan RA (2010) *Remote Sensing of  
Vegetation: Principles, Techniques and Applications*.  
OUP, Oxford
- Knorr W, Kaminski T, Scholze M, Gobron N, Pinty B,  
Giering R, Mathieu P-P (2010) Carbon cycle data  
assimilation with a generic phenology model.  
*J Geophys Res* 115, doi:10.1029/2009JG001119



- 2805 Knyazikhin YV, Marshak AL, Myneni RB (1992) 2859  
 2806 Interaction of photons in a canopy of finite dimen- 2860  
 2807 sional leaves. *Remote Sens Environ* 39:61–74 2861  
 2808 Knyazikhin YV, Kranigk J, Myneni RB, Panfyorov O, 2862  
 2809 Gravenhorst G (1998) Influence of small-scale 2863  
 2810 structure on radiative transfer and photosynthesis 2864  
 2811 in vegetation canopies. *J Geophys Res* 2865  
 2812 103:6133–6144 2866  
 2813 Knyazikhin YV, Schull MA, Liang X, Myneni RB, 2867  
 2814 Samanta A (2011) Canopy spectral invariants. Part 2868  
 2815 1: A new concept in remote sensing of vegetation. *J* 2869  
 2816 *Quant Spectrosc Radiat Transf* 112:727–735 2870  
 2817 Knyazikhin YV, Schull MA, Stenberg P, Möttus M, 2871  
 2818 Rautiainen M, Yang Y, Marshak A, . . . , Myneni 2872  
 2819 RB (2013) Hyperspectral remote sensing of 2873  
 2820 foliar nitrogen content. *Proc Natl Acad Sci USA* 2874  
 2821 110: E185–E192 2875  
 2822 Krieger G, Moreira A, Fiedler H, Hajnsek I, Werner M, 2876  
 2823 Younis M, Zink M (2007) TanDEM-X: A satellite 2877  
 2824 formation for high-resolution SAR interferometry. 2878  
 2825 *IEEE Trans Geosci Remote Sens* 45:3317–3341 2879  
 2826 Lafont S, Zhao Y, Calvet J-C, Peylin P, Ciais P, 2880  
 2827 Maignan F, Weiss M (2012) Modelling LAI, surface 2881  
 2828 water and carbon fluxes at high-resolution over 2882  
 2829 France: comparison of ISBA-A-gs and ORCHIDEE. 2883  
 2830 *Biogeosciences* 9:439–456 2884  
 2831 Lee J-E, Franksnberg C, van der Tol C, Berry JA, 2885  
 2832 Guanter L, Boyce CK, Fisher JB, . . . , Saatchi, S 2886  
 2833 (2013) Forest productivity and water stress 2887  
 2834 across Amazonia: observations from GOSAT chlo- 2888  
 2835 rophyll fluorescence. *Proc Royal Soc B* 2889  
 2836 280:1471–2954 2890  
 2837 Leersnijder RP (1992) PINOGRAM: A Pine Growth 2891  
 2838 Area Model. WAU dissertation 1499, Wageningen 2892  
 2839 Agricultural University, The Netherlands 2893  
 2840 Lefsky MA, Cohen WB, Parker GG, Harding DJ 2894  
 2841 (2002) Lidar remote sensing for ecosystem studies. 2895  
 2842 *Biogeosciences* 52:19–30 2896  
 2843 Lefsky MA, Harding DJ, Keller M, Cohen WB, 2897  
 2844 Carabajal CC, Espirito-Santo FDB, Hunter MO, de 2898  
 2845 Oliveira R Jr (2005) Estimates of forest canopy 2899  
 2846 height and aboveground biomass using ICESat. 2900  
 2847 *Geophys Res Lett* 32:L22S02 2901  
 2848 Lewis P (1999) Three-dimensional plant modelling for 2902  
 2849 remote sensing simulation studies using the Botani- 2903  
 2850 cal Plant Modelling System (BPMS). *Agron Agric* 2904  
 2851 *Environ* 19:185–210 2905  
 2852 Lewis P, Disney MI (1998) The botanical plant 2906  
 2853 modeling system (BPMS): a case study of multiple 2907  
 2854 scattering in a barley canopy. In: *Proceedings of* 2908  
 2855 *IGARSS'98*, Seattle, USA. 2909  
 2856 Lewis P, Disney MI (2007) Spectral invariants and 2910  
 2857 scattering across multiple scales from within-leaf 2911  
 2858 to canopy. *Remote Sens Environ* 109:196–206 2912  
 Lewis P, Gómez-Dans J, Kaminski T, Settle J, Quaife T, 2859  
 Gobron N, Styles J, Berger M (2012) An Earth 2860  
 Observation Land Data Assimilation System 2861  
 (EO-LDAS). *Remote Sens Environ* 120:219–235 2862  
 Liang S (2004) *Quantitative Remote Sensing of Land* 2863  
 Surfaces. Wiley, New York 2864  
 Lynch C (2008) Big data: How do your data grow? 2865  
*Nature* 455:28–29 2866  
 Maas HG, Bientert A, Scheller S, Keane E (2008) 2867  
 Automatic forest inventory parameter determined 2868  
 from terrestrial laser scanner data. *Int J Remote* 2869  
 Sens 29:1579–1593 2870  
 Malenovsky Z, Mishra KB, Zemek F, Rascher U, 2871  
 Nedbal L (2009) Scientific and technical challenges 2872  
 in remote sensing of plant canopy reflectance and 2873  
 fluorescence. *J Exp Bot* 60:2987–3004 2874  
 Mallet C, Bretar F (2009) Full-waveform topographic 2875  
 lidar: state-of-the-art. *ISPRS J Photogramm Remote* 2876  
 Sens 64:1–16 2877  
 Marshak A, Knyazikhin YV, Chiu JC, Wiscombe WJ 2878  
 (2011) Spectrally invariant approximation 2879  
 within atmospheric radiative transfer. *J Atmos Sci* 2880  
 68:3094–3111 2881  
 Martin G, Josserand SA, Bornman JF, Vogelmann TC 2882  
 (1989) Epidermal focussing and the light microen- 2883  
 vironment within leaves of *Medicago sativa*. *Physiol* 2884  
 Plant 76:485–492 2885  
 Meador I, Weaver WR (1980) Two-stream 2886  
 approximations to radiative transfer in planetary 2887  
 atmospheres: a unified description of existing 2888  
 methods and new improvements. *J Atmos Sci* 2889  
 37:630–643 2890  
 Mêch R, Prusinkiewicz P (1996) Visual models of 2891  
 plants interacting with their environment. 2892  
*Proceedings of SIGGRAPH 96*. New Orleans, 2893  
 Louisiana, August 4–9 1996. In computer graphics 2894  
 proceedings, annual conference series, ACM 2895  
 SIGGRAPH, pp 397–410 2896  
 Melamed NT (1963) Optical properties of powders. 2897  
 Part I. Optical absorption coefficients and the 2898  
 absolute value of the diffuse reflectance. Part 2899  
 II. Properties of luminescent powders. *J Appl Phys* 2900  
 34:560–570 2901  
 Mercado LM, Bellouin NM, Sitch S, Boucher O, 2902  
 Huntingford C, Wild M, Cox PM (2009) Impact 2903  
 of changes in diffuse radiation on the global land 2904  
 carbon sink. *Nature* 458:1014–1018 2905  
 Middleton E, Corp LA, Campbell PKE (2008) 2906  
 Comparison of measurements and FluorMOD 2907  
 simulations for solar-induced chlorophyll fluores- 2908  
 cence and reflectance of a corn crop under nitrogen 2909  
 treatments. *Int J Remote Sens* 29:5193–5213 2910  
 Miller J, Berger M, Goulas Y, Jacquemoud S, Louis J, 2911  
 Mohammed G, Moise N, . . . , Zarco-Tejada P (2005) 2912







- 2913 Development of a vegetation fluorescence canopy  
2914 model, ESTEC Contract No. 16365/02/NL/FF Final  
2915 Report
- 2916 Mitchard ETA, Saatchi SS, Woodhouse IR, Feldpausch  
2917 TR, Lewis SL, Sonké B, Rowland C, Meir P (2011)  
2918 Measuring biomass changes due to woody  
2919 encroachment and deforestation/degradation in a  
2920 forest-savanna boundary region of central Africa  
2921 using multi-temporal L-band radar backscatter.  
2922 *Remote Sens Environ* 115:2861–2873
- 2923 Monsi M, Saeki T (1953) Über den Lichtfaktor in den  
2924 Pflanzengesellschaften und seine Bedeutung für die  
2925 Stoffproduktion. *Jpn J Bot* 14:22–52
- 2926 Monteith JL, Unsworth MH (2008) Principles of Envi-  
2927 ronmental Physics, 3rd edn. Academic, Burlington
- 2928 Morsdorf F, Nichol C, Malthus T, Woodhouse IH  
2929 (2009) Assessing forest structural and physiological  
2930 information content of multi-spectral LiDAR  
2931 waveforms by radiative transfer modelling. *Remote*  
2932 *Sens Environ* 113:2152–2163
- 2933 Morton DC, Nagol J, Carbal J, Rosette J, Palace M,  
2934 Cook BD, Vermote EF, . . . , North PRJ (2014)  
2935 Amazon forests maintain consistent canopy struc-  
2936 ture and greenness during the dry season. *Nature*  
2937 506:221–224
- 2938 Moya I, Camenen L, Evain S, Goulas Y, Cerovic ZG,  
2939 Latouche L, Flexas J (2004) A new instrument for  
2940 passive remote sensing: 1. Measurement of sunlight-  
2941 induced chlorophyll fluorescence. *Remote Sens*  
2942 *Environ* 91:186–197
- 2943 Myneni RB, Ross J (eds) (1990) Photon-vegetation  
2944 Interactions: Applications in Optical Remote Sens-  
2945 ing and Plant Ecology. Springer, Heidelberg
- 2946 Myneni RB, Williams DL (1994) On the relationship  
2947 between fAPAR and NDVI. *Remote Sens Environ*  
2948 49:200–211
- 2949 Myneni RB, Ross J, Asrar G (1989) A review of the  
2950 theory of photon transport in leaf canopies. *Agric*  
2951 *For Meteorol* 45:1–153
- 2952 Myneni RB, Asrar G, Gerstl SAW (1990) Radiative  
2953 transfer in three-dimensional leaf canopies. *Transp*  
2954 *Theor Stat Phys* 19:205–250
- 2955 Myneni RB, Keeling CD, Tucker CJ, Asrar G, Nemani  
2956 RR (1997a) Increased plant growth in the northern  
2957 high latitudes from 1981 to 1991. *Nature* 386:698–702
- 2958 Myneni RB, Nemani RR, Running SW (1997b) Esti-  
2959 mation of global leaf area index and absorbed par  
2960 using radiative transfer models. *IEEE Trans Geosci*  
2961 *Remote Sens* 35:1380–1393
- 2962 Myneni RB, Hofmann S, Knyazikhin Y, Privette JL,  
2963 Glassy J, Tian J, Song X, . . . , Running SW (2002)  
2964 Global products of vegetation leaf area and fraction  
2965 absorbed PAR from year one of MODIS data.  
2966 *Remote Sens Environ* 83:214–231
- Myneni RB, Yang W, Nemani R., Huete AR, 2967  
Dickinson RE, Knyazikhin Y, Didan K, . . . , 2968  
Salomonson V (2007) Large seasonal swings in 2969  
leaf area of Amazon rainforests. *Proc Natl Acad* 2970  
*Sci USA* 104:4820–4823 2971
- Næsset E, Gobakken T, Holmgren J, Hyyppä H, 2972  
Hyyppä J, Maltamo M, Nilsson M, . . . , Söderman 2973  
U (2004) Laser scanning of forests: the Nordic 2974  
experience. *Scand J For Res* 19:482–499 2975
- Nagai S, Saigusa N, Muraoka H, Nasahara KN (2010) 2976  
What makes the satellite-based EVI-GPP relation- 2977  
ship unclear in a deciduous broad-leaved forest? 2978  
*Ecol Res* 25:359–365 2979
- Nicodemus FE, Richmond JC, Hsia JJ, Ginsberg IW, 2980  
Limperis T (1977) Geometrical considerations and 2981  
nomenclature for reflectance. NBS Monograph 2982  
160, National Bureau of Standards, U.S. Department 2983  
of Commerce, Washington, DC 2984
- Niinemets Ü, Anten NPR (2009) Packing the photo- 2985  
synthetic machinery: from leaf to canopy. In: 2986  
Laisk A, Nedbal L, Govindjee (eds) Photosynthesis 2987  
in Silico: Understanding Complexity from 2988  
Molecules to Ecosystems. Springer, Dordrecht, pp 2989  
363–399 2990
- Nilson T, Kuusk A (1989) A reflectance model for the 2991  
homogenous plant canopy and its inversion. *Remote* 2992  
*Sens Environ* 27:157–167 2993
- Norman JM, Miller EE, Tanner CB (1971) Light 2994  
intensity and sunfleck size distribution in plant 2995  
communities. *Agron J* 63:743–748 2996
- North PRJ (1996) Three-dimensional forest light inter- 2997  
action model using a Monte Carlo method. *IEEE* 2998  
*Trans Geosci Remote Sens* 34:946–956 2999
- Olioso A, Méthy M, Lacaze B (1992) Simulation of 3000  
canopy fluorescence as a function of canopy struc- 3001  
ture and leaf fluorescence. *Remote Sens Environ* 3002  
41:239–247 3003
- Olioso A, Inoue Y, Ortega-Farias S, Demarty J, 3004  
Wigneron JP, Braud I (2005) Future directions for 3005  
advanced evapotranspiration modeling: Assimilation 3006  
of remote sensing data into crop simulation models 3007  
and SVAT models. *Irrig Drain Syst* 19:377–412 3008
- Ollinger SV (2011) Sources of variability in canopy 3009  
reflectance and the convergent properties of plants. 3010  
*New Phytol* 189:375–394 3011
- Ollinger SV, Richardson AD, Martin ME, Hollinger DY, 3012  
Frolking SE, Reich PB, Plourde LC, . . . , Schmid HP 3013  
(2008) Canopy nitrogen, carbon assimilation, and 3014  
albedo in temperate and boreal forests: Functional 3015  
relations and potential climate feedbacks. *Proc Natl* 3016  
*Acad Sci USA* 105:19336–19341 3017
- Perttunen J, Sievänen R, Nikinmaa E (1998) 3018  
LIGNUM: a model combining the structure and 3019  
the functioning of trees. *Ecol Model* 108:189–198 3020

- 3021 Pettorelli N (2013) The Normalized Difference Vegeta- 3074  
 3022 tion Index. OUP, Oxford. ISBN 978-0-19-969316-0 3075  
 3023 Pettorelli N, Vik JO, Mysterud A, Gaillard J-M, 3076  
 3024 Tucker CJ, Stenseth NC (2005) Using the satellite- 3077  
 3025 derived NDVI to assess ecological responses to 3078  
 3026 environmental change. *Trend Ecol Evol* 20:503–510 3079  
 3027 Pfeifer M, Disney MI, Quaife T, Marchant R (2012) 3080  
 3028 Terrestrial ecosystems from space: a review of earth 3081  
 3029 observation products or macroecology applications. 3082  
 3030 *Glob Ecol Biogeogr* 21:603–624  
 3031 Pinty B, Verstraete MM, Dickinson RE (1989) 3083  
 3032 A physical model for predicting bidirectional 3084  
 3033 reflectances over bare soil. *Remote Sens Environ* 3085  
 3034 27:273–288 3086  
 3035 Pinty B, Gobron N, Widlowski J-L, Lavergne T, 3087  
 3036 Verstraete MM (2004) Synergy between 1-D and 3088  
 3037 3-D radiation transfer models to retrieve vegetation 3089  
 3038 canopy properties from remote sensing data. *J* 3090  
 3039 *Geophys Res* 109: D21205 3091  
 3040 Pinty B, Lavergne T, Dickinson R, Widlowski J-L, 3092  
 3041 Gobron N, Verstraete MM (2006) Simplifying the 3093  
 3042 interaction of land surfaces with radiation for relat- 3094  
 3043 ing remote sensing products to climate models. *J* 3095  
 3044 *Geophys Res* 111: D02116 3096  
 3045 Pinty B, Andredakis I, Clerici M, Kaminski T, 3097  
 3046 Taberner M, Verstraete MM, Gobron N, . . . , 3098  
 3047 Widlowski JL (2011a) Exploiting the MODIS 3099  
 3048 albedos with the Two-stream Inversion Package 3100  
 3049 (JRC-TIP). 1. Effective leaf area index, vegetation, 3101  
 3050 and soil properties. *J Geophys Res* 116:D09105 3102  
 3051 Pinty B, Andredakis I, Clerici M, Kaminski T, 3103  
 3052 Taberner M, Verstraete MM, Gobron N, . . . , 3104  
 3053 Widlowski JL (2011b) Exploiting the MODIS 3105  
 3054 albedos with the Two-stream Inversion Package 3106  
 3055 (JRC-TIP): 2. Fractions of transmitted and absorbed 3107  
 3056 fluxes in the vegetation and soil layers. *J Geophys* 3108  
 3057 *Res* 116:D09106 3109  
 3058 Prusinkiewicz P, Lindenmayer A (1990) *The Algorithmic* 3110  
 3059 *Beauty of Plants*. Springer, New York 3111  
 3060 Qin J, Liang S, Liu R, Zhang H, Hu B (2007) A weak- 3112  
 3061 constraint-based data assimilation scheme for 3113  
 3062 estimating surface turbulent fluxes. *IEEE Geosci* 3114  
 3063 *Remote Sens Lett* 4:649–653 3115  
 3064 Quaife T, Lewis P, De Kauwe M, Williams M, 3116  
 3065 Law BE, Disney MI (2008) Assimilating canopy 3117  
 3066 reflectance data into an ecosystem model with an 3118  
 3067 Ensemble Kalman Filter. *Remote Sens Environ* 3119  
 3068 112:1347–1364 3120  
 3069 Raunonen P, Kaasalainen M, Åkerblom M, 3121  
 3070 Kaasalainen S, Kaartinen H, Vastaranta M, 3122  
 3071 Holopainen M, . . . , Lewis P (2013) Comprehensive 3123  
 3072 quantitative tree models from terrestrial laser scan- 3124  
 3073 ner data. *Remote Sens* 5:491–520 3125  
 Rautiainen M, Stenberg P (2005) Application of pho- 3074  
 ton recollision probability in coniferous canopy 3075  
 reflectance model. *Remote Sens Environ* 96:98–107 3076  
 Richardson AD, Anderson RS, Arain MA, Barr AG, 3077  
 Bohrer G, Chen G, Chen JM, . . . , Xue Y (2012) 3078  
 Terrestrial biosphere models need better representa- 3079  
 tion of vegetation phenology: results from the North 3080  
 American Carbon Program Site Synthesis. *Glob* 3081  
*Chang Biol* 18:566–584 3082  
 Rosema A, Verhoef W, Schroote J, Snel JFH 3083  
 (1991) Simulating fluorescence light-canopy inter- 3084  
 action in support of laser-induced fluorescence 3085  
 measurements. *Remote Sens Environ* 37:117–130 3086  
 Rosette JAB, North PRJ, Suarez JC (2005) Vegetation 3087  
 height estimates for a mixed temperate forest using 3088  
 satellite laser altimetry. *Int J Remote Sens* 3089  
 29:1475–1493 3090  
 Ross JK (1981) *The Radiation Regime and The Archi-* 3091  
*tecture of Plant Stands*. Dr. W. Junk Publ, The Hague 3092  
 Ross JK, Marshak AL (1989) The influence of leaf 3093  
 orientation and the specular component of leaf 3094  
 reflectance on the canopy bidirectional reflectance. 3095  
*Remote Sens Environ* 27:251–260 3096  
 Saatchi SS, Harris N, Brown S, Lefsky M, Mitchard E, 3097  
 Salas W, Zutta B, . . . , Morel A (2011) Benchmark 3098  
 map of forest carbon stocks in tropical regions 3099  
 across three continents. *Proc Natl Acad Sci USA*, 3100  
 108:9899–9904 3101  
 Saleska SR, Didan K, Huete AR, da Rocha HR (2007) 3102  
 Amazon forests green-up during 2005 drought. *Sci-* 3103  
*ence* 318:612 3104  
 Samanta A, Ganguly S, Hashimoto H, Devadiga S, 3105  
 Vermote E, Knyazikhin Y, Nemani RR, Myneni, 3106  
 RB (2010) Amazon forests did not green-up during 3107  
 the 2005 drought. *Geophys Res Lett* 37: L05401 3108  
 Schaepman-Strub G, Schaepman ME, Painter TH, 3109  
 Dangel S, Martonchik JV (2006) Reflectance 3110  
 quantities in optical remote sensing – definitions 3111  
 and case studies. *Remote Sens Environ* 103:27–42 3112  
 Schull MA, Knayzikhin YV, Xu L, Samanta A, 3113  
 Carmona PL, Lepine L, Jenkins JP, . . . , Myneni 3114  
 RB (2011) Canopy spectral invariants, Part 2: Appli- 3115  
 cation to classification of forest types from 3116  
 hyperspectral data. *J Quant Spectrosc Radiat Transf* 3117  
 112:736–750 3118  
 Sellers PJ (1985) Canopy reflectance, photosynthesis 3119  
 and transpiration. *Int J Remote Sens* 6:1335–1372 3120  
 Sitch S, Smith B, Prentice IC, Arneth A, Bondeau A, 3121  
 Cramer W, Kaplan JO, . . . , Venevsky S (2003) 3122  
 Evaluation of ecosystem dynamics, plant geography 3123  
 and terrestrial carbon cycling in the LPJ dynamic 3124  
 global vegetation model. *Glob Chang Biol* 3125  
 9:161–185 3126

- 3127 Sivia D, Skilling J (2006) *Data Analysis: A Bayesian*  
3128 *Tutorial*, 2nd edn. Oxford University Press, Oxford
- 3129 Smolander S, Stenberg P (2005) Simple parameter-  
3130 izations of the radiation budget of uniform  
3131 broadleaved and coniferous canopies. *Remote Sens*  
3132 *Environ* 94:355–363
- 3133 Solomon SD, Qin M, Manning M, Chen M, Marquis  
3134 MB, Averyt M, Tignor M, Miller HL (eds) (2007)  
3135 Contribution of Working Group I to the Fourth  
3136 Assessment Report of the Intergovernmental Panel  
3137 on Climate Change, 2007
- 3138 Strahler AH (1996) Vegetation canopy reflectance  
3139 modeling: recent developments and remote sensing  
3140 perspectives. *Remote Sens Rev* 15:179–194
- 3141 Tang H, Dubayah R, Swatantran A, Hofton M,  
3142 Sheldon S, Clark D, Blair B (2012) Retrieval of  
3143 vertical LAI profiles over tropical rain forests  
3144 using waveform lidar at La Selva, Costa Rica.  
3145 *Remote Sens Environ* 124:242–250
- 3146 Tarantola A (2005) *Inverse Problem Theory and*  
3147 *Methods for Model Parameter Estimation*, Society  
3148 for the Industrial and Applied Mathematics (SIAM),  
3149 Philadelphia, PA
- 3150 Twomey S (1977) *Introduction to the Mathematics*  
3151 *of Inversion in Remote Sensing and Indirect*  
3152 *Measurements*. Elsevier, Amsterdam
- 3153 Ustin S (2013) Remote sensing of canopy chemistry.  
3154 *Proc Natl Acad Sci USA* 110: 804–805
- 3155 Vargas I, Niklasson GA (1997) Applicability  
3156 conditions of the Kubelka-Munk theory. *Appl Opt*  
3157 36:5580–5586
- 3158 Verhoef W (1984) Light-scattering by leaf layers with  
3159 application to canopy reflectance modeling – the  
3160 SAIL model. *Remote Sens Environ* 16:125–141
- 3161 Verstraete MM, Pinty B, Myneni RB (1996) Potential  
3162 and limitations for information extraction from  
3163 remote sensing. *Remote Sens Environ* 58:201–214
- 3164 Wang WM, Li ZL, Su HB (2007) Comparison of leaf  
3165 angle distribution functions: effects on extinction  
3166 coefficient and fraction of sunlit foliage. *Agric For*  
3167 *Meteorol* 143:106–122
- 3168 Wanner W, Strahler AH, Hu B, Lewis P, Muller JP,  
3169 Li X, Barker-Schaaf CL, Barnsley MJ (1997) Global  
3170 retrieval of bidirectional reflectance and albedo over  
3171 land from EOS MODIS and MISR data: theory and  
3172 algorithm. *J Geophys Res* 102:17143–17161
- 3173 Widlowski JL, Lavergne T, Pinty B, Verstraete MM,  
3174 Gobron N (2006) Rayspread: A virtual laboratory for  
3175 rapid BRF simulations over 3-D plant canopies. In:  
3176 Frank G (ed) *Computational Methods in Transport*,  
3177 *Lecture Notes in Computational Science and Engi-*  
3178 *neering Series*, 48. Springer, Berlin, pp 211–231
- Widlowski JL, Taberner M, Pinty B, Bruniquel-Pinel V, 3179  
Disney MI, Fernandes R, Gastellu-Etcheberry 3180  
JP, . . . , Xie D (2007) The third Radiation transfer 3181  
Model Intercomparison (RAMI) exercise: Document- 3182  
ing progress in canopy reflectance modelling, 3183  
*J Geophys Res* 112: D09111 3184
- Widlowski JL, Robustelli M, Disney MI, Gastellu- 3185  
Etcheberry JP, Lavergne T, Lewis P, North PRJ, . . . , 3186  
Verstraete MM (2008) The RAMI On-line Model 3187  
Checker (ROMC): A web-based benchmarking facil- 3188  
ity for canopy reflectance models. *Remote Sens Envi-* 3189  
ron 112:1144–1150 3190
- Widlowski JL, Pinty B, Clerici M, Dai Y., De 3191  
Kauwe M, de Ridder K, Kallel A, . . . , Yuan H 3192  
(2011) RAMI4PILPS: An intercomparison of 3193  
formulations for the partitioning of solar radiation 3194  
in land surface models. *J Geophys Res* 116: 3195  
G02019, 25 3196
- Widlowski JL, Pinty B, Lopatka M, Aytzberger C, 3197  
Buzica D, Chelle M, Disney MI, . . . , Xie D (2013) 3198  
The fourth Radiation transfer Model Intercompari- 3199  
son (RAMI-IV): Proficiency testing of canopy 3200  
reflectance models with ISO-13528, *J Geophys Res* 3201  
118:1–22 3202
- Woodhouse IH, Nichol C, Sinclair P, Jack J, 3203  
Morsdorf F, Malthus TJ, Patenaude G (2011) A 3204  
multispectral canopy LiDAR demonstrator project. 3205  
*IEEE Geosci Remote Sens Lett* 8:839–843 3206
- Woodhouse IH, Mitchard ETA, Brolly M, Maniatis D, 3207  
Ryan CM (2012) Radar backscatter is not a ‘direct 3208  
measure’ of forest biomass. *Nat Clim Change* 3209  
2:556–557 3210
- Wulder M, White J, Nelson R, Næsset E, Ørka H, 3211  
Coops N, Hilker T, . . . , Gobakken T (2012) Lidar 3212  
sampling for large-area forest characterization: A 3213  
review. *Remote Sens Environ* 121:196–209 3214
- Yao T, Yang X, Zhao F, Wang Z, Zhang Q, Jupp D, 3215  
Lovell J, . . . , Strahler A (2011) Measuring forest 3216  
structure and biomass in New England forest stands 3217  
using Echidna ground-based lidar. *Remote Sens* 3218  
*Environ* 115:1144–1150 3219
- Zarco-Tejada P, Miller JR, Pedros R, Verhoef W, 3220  
Berger M (2006) FluorMODgui V3.0: a graphic 3221  
user interface for the spectral simulation of leaf 3222  
and canopy chlorophyll fluorescence. *Comput* 3223  
*Geosci* 32:577–591 3224
- Zarco-Tejada PJ, Bernia JAJ, Suárez L, Sepulcre- 3225  
Cantó G, Morales F, Miller JR (2009) Imaging chlo- 3226  
rophyll fluorescence with an airborne narrow-band 3227  
multispectral camera for vegetation stress detection. 3228  
*Remote Sens Environ* 113:1262–1275 3229

# Author Queries

Chapter No.: 11      0002576192

Queries	Details Required	Author's response
AU1	References Pettorelli et al. (2013), Goel (1989), Lewis (2007), Kubelka and Munk (1931), Suits (1972), Hapke (1981), Verstraete et al. (1990), Govaerts (1996), Knorr and Heimann (2001), Rodell et al. (2004), Dubayah et al. (2010), Disney et al. (2014), Lee and Pottier (2009), Schreiber et al. (1994), Baker (2008), Meroni et al. (2009) are cited in text but not given in the reference list. Please provide details in the list or delete the citations from the text.	
AU2	Reference citations Knyazikhin et al. (2012), Knorr et al. (2009), Mitchard et al. (2009) have been changed to Knyazikhin et al. (2013), Knorr et al. (2010), Mitchard et al. (2011) respectively as per the reference list. Please check if okay.	
AU3	Please provide opening parenthesis in sentence "For real canopies the exponent . . ."	
AU4	Please check " $\sim 10^1$ km" for correctness.	
AU5	Please provide in-text citation for references Best et al. (2011), Dickinson (1983), Disney et al. (2005), Grace et al. (2007), Meador and Weaver (1980), Myneni et al. (2002), Myneni and Williams (1994), Myneni et al. (1997), Myneni et al. (2007), Nagai et al. (2010), Ollinger et al. (2008), Ross and Marshak (1989), Sellers (1985), Sitch et al. (2003), Solomon et al. (2007), Wulder et al. (2012).	
AU6	Please confirm the updated author name in the reference Brut et al. (2009).	
AU7	Please confirm the inserted publisher location for the references Houser et al. (1995), Niinemets and Anten (2009), Ross (1981).	